ESTIMATION OF EJECTION FRACTIONS BY THREE QUANTITATIVE GATED SPECT SOFTWARE PACKAGES

ORANUCH TIAPETCH

A THESIS SUBMITTED IN PARTIAL FULFILLMENT
OF THE REQUIREMENTS FOR
THE DEGREE OF MASTER OF SCIENCE
(MEDICAL PHYSICS)
FACULTY OF GRADUATE STUDIES
MAHIDOL UNIVERSITY
2006

ISBN 974-04-7079-3

Thesis

Entitled

ESTIMATION OF EJECTION FRACTIONS BY THREE QUANTITATIVE GATED SPECT SOFTWARE PACKAGES

Oranuch Tiapetch

Miss.Oranuch Tiapetch
Candidate

Chiraporn Tocharoenchai

Assoc.Prof.Chiraporn Tocharoenchai,
Ph.D. (Biomedical Engineering)
Major Advisor

Pawana Pusuwan

Assoc.Prof.Pawana Pusuwan,
M.D.
Co-Advisor

Prof. M.R. Jisnuson Svasti, Ph.D
Dean
Faculty of Graduate Studies

Assoc. Prof. Vipa Boonkitticharoen,
Ph.D. (Radiation Biology)
Chair
Master of Science Programme
In Medical Physics
Faculty of Medicine
Ramathibodi Hospital

Thesis

Entitled

ESTIMATION OF EJECTION FRACTIONS BY THREE QUANTITATIVE GATED SPECT SOFTWARE PACKAGES

was submitted to the Faculty of Graduate Studies, Mahidol University
for the degree of Master of Science (Medical Physics)
On
April 17, 2006

Miss.Oranuch Tiapetch
Candidate

Assoc.Prof.Chiraporn Tocharoenchai, Ph.D. (Biomedical Engineering)
Chair

Assoc.Prof.Tawatchai Chaiwatanarat, M.D.
Member

Assoc.Prof.Pawana Pusuwan, M.D.
Member

Prof. M.R. Jisnuson Svasti, Ph.D
Dean
Faculty of Graduate Studies
Mahidol University

Professor Rajata Rajatanavin, M.D., F.A.C.E.
Dean
Faculty of Medicine
Ramathibodi Hospital
Mahidol University

ACKNOWLEDGEMENTS

The success of this thesis can been attributed to the extensive support and assistance from my major advisor, Assoc.Prof.Chiraporn Tochareonchai, Faculty of Medical Technology, Mahidol University. She was always there to listen and to give advice. She taught me how to ask questions and express my ideas. I deeply thank her for their valuable advice and guidance in this research.

A special thanks goes to my co-advisor, Assoc.Prof.Pawana Pusuwan, Faculty of Medicine, Siriraj Hospital, who is most responsible for helping me complete the writing of this thesis. She was always there to meet and talk about my ideas, to proofread and mark up my chapters. Without her encouragement and constant guidance, I could not have finished this thesis.

Besides my advisors, I would like to thank my thesis committee, Assoc.Prof.Tawatchai Chaiwatanarat, Faculty of Mecicine, Chulalongkorn University, who asked me good questions, gave insightful comments and reviewed my work on a very short notice.

I would like to thank Suraphong Leaungwutiwong and staff of Section of Nuclear Medicine at Bumrungrad Hospital, for all the supports. I also thank Dr.Chulaluk Komoltri, Division of Clinical Epidemiology, Faculty of Medicine, Siriraj Hospital, for statistical suggestions.

I would like to thank Assoc.Prof.Vipa Boonkitticharoen, Chair of Science program in Medical Physics, Faculty of Medicine, Ramathibodi Hospital and the lecturers of Medical Physics program for their valuable advice.

Let me also “thank you” to staff and my friends in Medical Physics for their kind support.

Last, but not least, I thank my family for giving me life in the first place, for educating me with aspects from both arts and sciences, for unconditional support, entirely care and love.

Oranuch Tiapetch

ESTIMATION OF EJECTION FRACTIONS BY THREE QUANTITATIVE GATED SPECT SOFTWARE PACKAGES.

ORANUCH TIAPETCH 4637057 RAMP/M

M.Sc.(MEDICAL PHYSICS)

THESIS ADVISORS : CHIRAPORN TOCHAROENCHAI, Ph.D. (BIOMEDICAL ENGINEERING), PAWANA PUSUWAN, M.D.

ABSTRACT

The purposes of the study were to investigate the accuracy of left ventricular ejection fractions (LVEFs) estimated from three quantitative gated SPECT software packages, using echocardiography as a gold standard and the reliability of LVEF from ordered subset expectation maximization (OS-EM). Seventy patients with suspected coronary artery disease (CAD) were examined with gated ^{99m}Tc-MIBI SPECT (8 frames/cardiac cycle) at stress. The projection datasets were reconstructed using OS-EM with 8 angles/subset. The data were smoothed with gaussian filter with FWHM of 8 pixel width. The iteration numbers were varied for each software: 3 iterations for quantitative gated SPECT (QGS), 5 iterations for the Emory cardiac toolbox (ECTb), and 4 iterations for 4D-MSPECT. The LVEFs were calculated using these 3 quantitative software packages. To test reliability of LVEF from OS-EM, the same patient data were again reconstructed using filtered backprojection (FBP) with post-filtering of Butterworth 5th order, 0.3 cycles/pixel cutoff frequency. A two tailed pair t-test was used to test the statistically significant difference with p-value < 0.05. The results showed that there were no statistically significant differences in LVEFs for all three software packages from echocardiography with $p > 0.05$. The correlation between LVEF in each pair of package was high ($r > 0.9$). The LVEFs from OS-EM were not statistically significantly different from that from FBP ($p > 0.05$) for QGS and 4D-MSPECT, but for ECTb, there was a statistically significant difference. The LVEF from OS-EM correlated well with that from FBP ($r > 0.9$). The LVEF estimated from each software package had different characteristics and the LVEF from OS-EM was reliable.

KEY WORDS : EJECTION FRACTION / GATED SPECT / QGS / ECTb / 4D-MSPECT

74 P. ISBN 974-04-7079-3

การประเมินค่า EJECTION FRACTIONS ที่ได้จาก 3 โปรแกรม ที่ใช้ในการคำนวณเชิงปริมาณจาก GATED SPECT (ESTIMATION OF EJECTION FRACTIONS BY THREE QUANTITATIVE GATED SPECT SOFTWARE PACKAGES)

อรนุช เตียะเพชร 4637057 RAMP/M
วท.ม. (ฟิสิกส์การแพทย์)

คณะกรรมการควบคุมวิทยานิพนธ์ : จิราภรณ์ โตเจริญชัย, Ph.D. (Biomedical Engineering), ภาวนา ภูสุวรรณ, พ.บ.ว.ว.(รังสีวิทยาทั่วไป)

บทคัดย่อ

วัตถุประสงค์ของการศึกษาวิจัยเพื่อประเมินความถูกต้องของค่า left ventricular ejection fraction (LVEFs) ที่ได้จาก 3 โปรแกรม ที่ใช้ในการคำนวณเชิงปริมาณจาก gated SPECT โดยใช้ผลจากการตรวจหัวใจด้วยอัลตราซาวด์เป็นมาตรฐาน และเพื่อศึกษาความน่าเชื่อถือของค่า LVEF จากการสร้างภาพแบบ OS-EM ซึ่งได้ทำการศึกษาในผู้ป่วยจำนวน 70 ราย ที่มีประวัติสงสัยว่าเป็นโรคหลอดเลือดหัวใจโคโรนารีย์ ผู้ป่วยแต่ละรายจะได้รับการตรวจโดยใช้ ^{99m}Tc-MIBI เก็บข้อมูลแบบ gated โดยใช้ 8 frames/cardiac cycle ที่สภาวะ stress จากนั้นทำการสร้างภาพแบบ OS-EM ซึ่งใช้ 8 angles/subset ภาพที่ได้จะถูกทำให้ smooth ด้วย gaussian filter ที่ FWHM เท่ากับ 8 pixel ส่วนจำนวนรอบที่ใช้ในการสร้างภาพสำหรับแต่ละโปรแกรมนั้นจะแตกต่างกันดังนี้ โปรแกรม QGS ใช้ 3 รอบ, โปรแกรม ECTb ใช้ 5 รอบ และโปรแกรม 4D-MSPECT ใช้ 4 รอบ จากนั้นจึงทำการคำนวณหาค่า LVEFs จากทั้ง 3 โปรแกรม และเพื่อทดสอบความน่าเชื่อถือของค่า LVEF จากการสร้างภาพแบบ OS-EM ข้อมูลจากผู้ป่วยในชุดเดียวกันจะถูกสร้างภาพใหม่โดยใช้ FBP ทำการขจัด noise โดยใช้ Butterworth filter ที่ order = 5 และ cutoff frequency = 0.3 cycles/pixel สำหรับการทดสอบทางสถิตินั้น จะใช้ pair t-test เพื่อทดสอบความแตกต่างของผลที่ได้แต่ละคู่ โดยถ้าค่า $p < 0.05$ แสดงว่าความแตกต่างนั้นมีนัยสำคัญทางสถิติ ผลการศึกษาพบว่าค่า LVEFs ที่คำนวณได้จากทั้งสามโปรแกรมเมื่อเทียบกับผลจากอัลตราซาวด์ไม่แตกต่างกันด้วยค่า $p > 0.05$ และความสัมพันธ์ของ LVEF ระหว่างโปรแกรมแต่ละคู่นั้นมีค่าสูง ($r > 0.9$) ในโปรแกรม QGS และ 4D-MSPECT นั้นพบว่า การสร้างภาพแบบ OS-EM ให้ค่า LVEF ไม่ต่างจากการสร้างภาพแบบ FBP ($p > 0.05$) แต่ในโปรแกรม ECTb พบว่าค่าที่ได้จากการสร้างภาพทั้งสองวิธีนั้นต่างกันอย่างมีนัยสำคัญทางสถิติ และค่า LVEF จากการสร้างภาพแบบ OS-EM มีความสัมพันธ์สูงกับ FBP ($r > 0.9$) จากผลการศึกษาจะเห็นได้ว่าค่า LVEF ที่คำนวณได้จากแต่ละโปรแกรมมีคุณลักษณะเฉพาะตัวที่ต่างกันและค่า LVEF ที่ได้จากการสร้างภาพแบบ OS-EM มีความน่าเชื่อถือ

74 หน้า . ISBN 974-04-7079-3

CONTENTS

LIST OF TABLES

LIST OF FIGURES

LIST OF FIGURES (Continued)

LIST OF FIGURES (Continued)

LIST OF FIGURES (Continued)

LIST OF FIGURES (Continued)

LIST OF ABBRAVIATIONS

Abbreviation	Term
1D	one dimension
2D	two dimension
3D	three dimension
4D	four dimention
CAD	coronary artery disease
CI	confidence interval
COM	center of mass
CT	computed tomography
EBCT	electron-beam computed tomography
ECG	electrocardiogram
ECTb	Emory cardiac toolbox
ED	end-diastole
EDV	end-diastolic volume
EF	ejection fraction
ES	end-systole
ESV	end-systolic volume
FBP	filtered backprojection
FPRNA	first-pass radionuclide angiography
FT	Fourier transform
FWHM	full-width-at-haft-maximum
GBP	gated blood pool
IV	intravenous
LA	long axis
LPO	left posterior oblique
LV	left ventricle
LVEF	left ventricular ejection fraction

LIST OF ABBREVIATIONS (Continued)

Abbreviation	Term
MDCT	multidetector computed tomography
ML-EM	maximum likelihood-expectation maximization
MRI	magnetic resonance imaging
OS-EM	ordered subset-expectation maximization
pFAST	perfusion and function analysis for gated SPECT
QGS	quantitative gated SPECT
RAO	right anterior oblique
SA	short axis
SNR	signal-to-noise ratio
SPECT	single photon emission tomography
TEE	transesophageal echocardiogram
TTE	transthoracic echocardiogram

CHAPTER I
INTRODUCTION

The left ventricular (LV) functions, or myocardial perfusion, has major diagnostic and prognostic importances in patients with coronary artery disease (CAD) (1). Myocardial perfusion study is widely used for assessment of blood flow to the heart muscle whereas equilibrium gated blood pool is the widely used for assessment of ventricular functions such as ejection fraction (EF), ventricular volume, and regional wall motion. Early nuclear cardiology, the assessment of the myocardial perfusion was separated from ventricular functions. Recently, the development of myocardial gated SPECT has allowed simultaneous assessment of myocardial perfusion and ventricular function from a single procedure. This development has accelerated the utilization of this procedure for the diagnosis and prognosis associated with CAD (2). Myocardial gated SPECT is now routinely used to assess, in addition to myocardial perfusion, global and regional left ventricular functions. The main parameter of global function that is measured is left ventricular ejection fraction (LVEF) (3).

For quantitative analysis of left ventricle, several kinds of gated SPECT software have been developed and applied to clinical practice. The three most widely distributed software packages available in nuclear medicine are quantitative gated SPECT (QGS, Cedars-Sinai Medical Center, Los Angeles, CA), the Emory Cardiac Toolbox (ECTb, Emory University, Atlanta, GA) and 4D-MSPECT (University of Michigan Medical Center, Ann Arbor, MI). All of these software packages have been validated for LVEF calculation. Several publications have established agreement between LVEF estimated from gated SPECT and those from other methods such as echocardiography, equilibrium gated blood pool and magnetic resonance imaging (MRI) (4-7). Due to differences in methods used for left ventricle calculations, the ejection fractions (EFs) obtained from these three software packages are different, leading to problems in clinical applications. In this investigation, we studied the

accuracy of the ejection fractions obtained from these three software packages compared with that from echocardiography. Furthermore, left ventricular volume calculation is based on edge detection and geometric modeling of the heart. Image quality such as resolution and contrast also affects edge detection. Most of the studies determined the ejection fractions using those three packages using filtered backprojection (FBP) algorithm. Many studies also showed that iterative image reconstruction algorithm namely ordered subset expectation maximization (OS-EM) provided better image quality than FBP algorithm (8-10). Therefore, we studied the ejection fraction obtained from OS-EM compared with that from FBP.

CHAPTER II
OBJECTIVES

The objectives of this study are:

2.1 To study the accuracy of left ventricular ejection fractions estimated from three quantitative gated SPECT software packages.

2.2 To compare left ventricular ejection fractions obtained from ordered subset expectation maximization (OS-EM) and filtered backprojection (FBP).

CHAPTER III
BACKGROUND

Coronary artery disease (CAD) is the most common form of heart disease. It is the end result of the accumulation of atheromatous plaques (fatty deposit in the intima (inner lining) of an artery) within the walls of the arteries that supply the myocardium (the muscle of the heart). After decades of progression, some of these atheromatous plaques may rupture and (along with the activation of the blood clotting system) start limiting blood flow to the heart muscle. As the plaques grow in thickness and obstruct more than 70 percents of the diameter of the vessel, symptoms of obstructive coronary artery disease have been developed. At this stage of the disease process, the patient can be said to have ischemic heart disease. As the degree of coronary artery disease progresses, there may be nearly complete obstruction of the lumen of the coronary artery, severely restricting the flow of oxygen-carrying blood to the myocardium. With this degree of coronary heart disease, patients typically have suffered from myocardial infarctions (heart attacks).

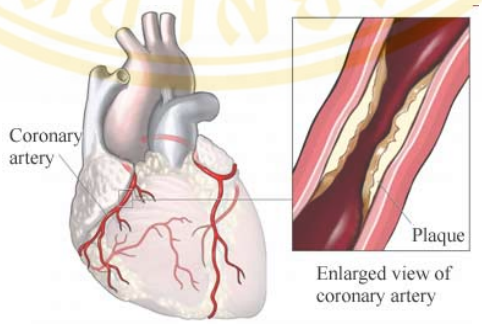

Figure 1. Heart and coronary artery (11)**.**

It is important to distinguish between myocardial ischemia and myocardial infarction. Ischemia means that the amount of oxygen supplied to the tissue is inadequate to supply the demands of the tissue. When large areas of the myocardium become ischemic, there can be impairment in the relaxation and contraction of the myocardium. If the blood flow to the tissue is improved, myocardial ischemia can be reversed. Infarction means that the tissue has undergone irreversible death due to lack of sufficient oxygen-rich blood (12).

In addition to a physical examination and blood chemistry, there are several tests recommended to evaluate coronary artery disease as follows.

3.1 Electrocardiogram (ECG)

An electrocardiogram, which is sometimes called an EKG, is a test that measures the electrical signals that control the rhythm of the heartbeat. During an electrocardiogram, the electrodes are attached to the skin on the chest, arms, and legs. The electrodes are also connected to a machine that translates the electrical activity into line tracings on paper (13). This test can show evidence of a previous heart attack or one that is in progress. It can also yield other useful information, such as the status of heart's electrical system. ECG readings taken continuously over a period of 24 hours or longer may help detect silent ischemia (14).

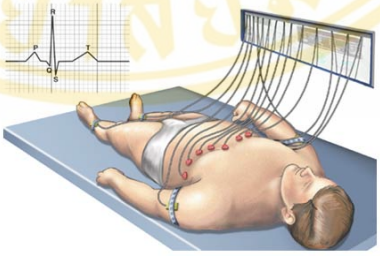

Figure 2. Electrod position and EKG (15).

3.2 Echocardiography

An echocardiogram or echo is a type of ultrasound test that uses high-pitched sound waves to produce an image of the heart. The sound waves are sent through a device called a transducer and are reflected off the various structures of the heart.

These echoes are converted into pictures of the heart that can be seen on a video monitor. An echocardiogram generally is used to evaluate heart wall thickness and motion, as well as the structure and function of the heart valves. It can also be used to estimate the amount of blood pumped out of left ventricle with each heartbeat (ejection fraction), previous injury to the heart muscle caused by impaired blood flow, or evidence of heart failure, especially in people with chest pain or a possible heart attack. In addition, an echocardiogram can detect a blood clot in the heart, evaluate the heart valves for abnormalities, and identify pericardial effusion. There are different types of echocardiograms; transthoracic echocardiogram (TTE) is the standard method most commonly used. Views of the heart are obtained by moving the transducer to different locations on the chest or abdominal wall. Transesophageal echocardiogram (TEE) is one of the tests that the transducer is passed down the esophagus instead of being moved over the outside of the chest wall. TEE shows clearer pictures, because the transducer is located closer to the heart and because the lungs and bones of the chest wall do not interfere with the sound waves produced by the transducer. Stress echocardiogram involves a transthoracic echocardiogram both before and after heart is stressed either by exercise or by drug (dobutamine) that makes the heart beat harder and faster. A stress echocardiogram is usually done to determine the flow of blood to the heart (coronary artery disease).

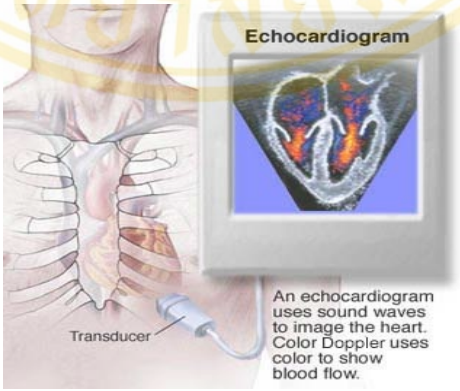

Figure 3. Echocardiogram (16).

3.3 Coronary angiography (or arteriography)

Cardiac catheterization is a test to image heart and coronary arteries. To perform cardiac catheterization, a thin flexible tube called a catheter is threaded through a blood vessel in the arm or groin and into the heart. Then a contrast material is injected into the coronary arteries to trace the movement of blood through the arteries via the catheter. The purpose of cardiac catheterization is to determine the size and location of plaque that may have built up in coronary arteries from atherosclerosis. This test gives an accurate result but it is invasive and costly.

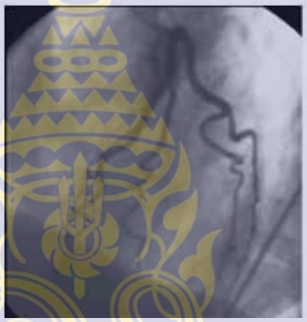

Figure 4. Coronary arteries image from coronary angiography (17).

3.4 Coronary magnetic resonance angiography

This test uses magnetic waves to produce a three-dimensional image of coronary arteries to check for narrowings or blockages. This test is still being developed, but it has the advantage of producing images of coronary arteries with a noninvasive procedure.

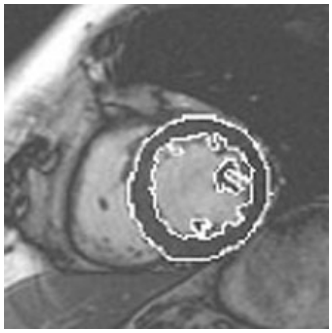

Figure 5. An example of transverse view of left ventricle from MRI (18).

3.5 Computed Tomography (CT)

A traditional CT scan is an x-ray procedure that combines many x-ray images with the aid of a computer to generate cross-sectional views of the body. Cardiac CT uses the advanced CT technology with intravenous (IV) contrast (dye) to visualize cardiac anatomy, coronary circulation and great vessels. In the past, CT was not routinely used for evaluation of the heart. This is primarily because, the scan times were not fast enough to image the heart without cardiac motion. The development of electron-beam computed tomography (EBCT) begun in the mid 1980s. The rapid scan rate helps freeze the cardiac motion. ECG triggering is added to synchronize cardiac phases from slice to slice. These features make EBCT suitable for cardiac imaging, however, EBCT is beset by limited x-ray-power output, such that scanning at top speed and thinnest slice in adults produces images with poor signal-to-noise ratio (SNR). Cardiac multidetector CT (MDCT) overcomes many shortcomings of EBCT. Technically, cardiac MDCT produces images with better SNR at a thinner slice thickness, although at a lower scan rate and increased radiation dose. It is expected that in the near future, MDCT will become the dominant CT modality for cardiac imaging. Although cardiac CT gives the image with high spatial resolution, but it exposes the patient to harmful ionizing radiation (19,20).

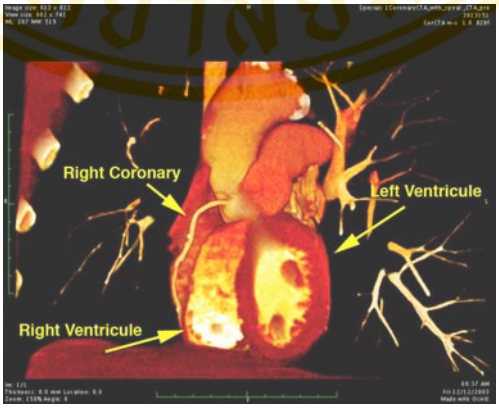

Figure 6. Heart and coronary arteries image from cardiac CT (21).

3.6 Nuclear cardiology

Nuclear cardiology includes an extensive range of investigations for the assessment of cardiac disease but the most important areas are the assessment of myocardial perfusion and measurement of ventricular functions. Myocardial perfusion studies are a widely utilized non-invasive imaging modality for the diagnosis and management of coronary artery disease whereas ventricular function studies are used to quantitative assessment of cardiac performance, for example, left ventricular ejection fraction, ventricular volume, myocardial wall motion and wall thickening, etc. These differ in radiopharmaceutical and imaging technique as described below:

3.6.1 Myocardial Perfusion Imaging

The purpose of myocardial perfusion imaging is to evaluate myocardial blood flow. The most popular radiopharmaceutical for myocardial perfusion imaging is technitium-99m sestamibi (^{99m}Tc-MIBI). It is a lipophilic compound that diffuses passively out of the blood and apparently localizes within the myocardial cell to mitochondrial membranes on the basis of its negative electrical potentials. The advantage of ^{99m}Tc-MIBI is long clearance half-time from the myocardium, in excess of 5 hours. This provides a window of several hours after tracer administration in which to accomplish imaging. In addition, technical advance of SPECT has been developed for three-dimensional displays that improved diagnostic results (22,23). The myocardial perfusion scan usually consists of two parts, after exercising (stress) and under resting conditions. These are based on the concept of coronary blood flow reserve. Under conditions of exercise, the oxygen demand of the myocardium increases in response to the increased cardiac workload. Normal coronary arteries, dilate and flow increase but stenosis vessels do not dilate; flow reserve is limited; myocardial ischemia is induced (24). A diagnostic scheme is presented in Table 1 that uses the appearance of the scintigrams on the rest and stress images to characterize ischemia and infarction. No evidence of CAD is diagnosed when the scintigrams at rest and stress are no defects as shown on the top row in Table 1. To be diagnosed as ischemic heart, the scintigrams show no defect at rest but at the same location there is defect at stress as shown on the middle row. On the bottom row, the scintigrams show

defect at the same location on both rest and stress study. This condition can be diagnosed as myocardial infarction.

- Image Acquisition

The patient lies on the imaging table in the supine position. Recently, dual-headed cameras in the 90-degree configuration have been preferred, as images can be acquired in half the time required using a single-headed system. A 180-degree imaging arc is usually obtained, scanning from the 45-degree right anterior oblique (RAO) to the 45-degree left posterior oblique (LPO) position (25), as shown in Figure 7.

Table 1. Diagnostic patterns; myocardial perfusion images after rest and stress testing. The arrow indicated the area of interest.

Diagnostic	Rest Study	Stress Study
Normal	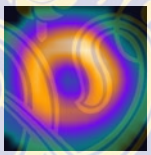 no defect	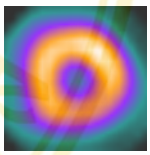 no defect
Ischemia	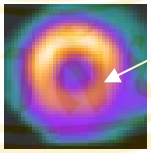 no defect	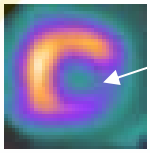 defect
Infarction	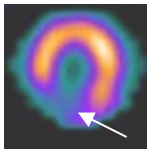 defect	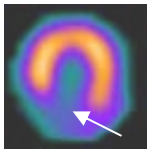 defect

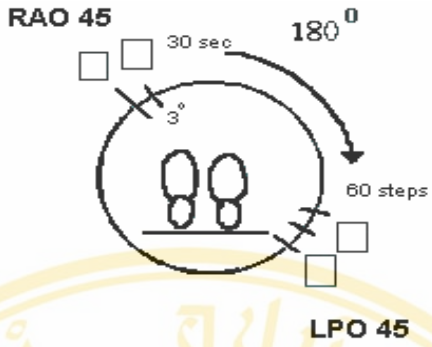

Figure 7. The example of myocardial SPECT acquisition, a 180-degree imaging arc scanned from 45° RAO to 45° LPO, 60 projection images are obtained (26).

3.6.2 Equilibrium Gated Blood Pool Imaging

Equilibrium gated blood pool study was first introduced in the early 1970s and was quickly established as the assessment of ventricular functions (27). Equilibrium imaging requires a radiopharmaceutical that is retained within the blood pool. Red blood cell are labeled with technetium-99m (^{99m}Tc-RBCs), allowed to distribute uniformly throughout the blood volume, and then imaged with a gamma camera.

- Image Acquisition

During the equilibrium gated blood pool scan, electrodes are placed on the patient's body so that an electrocardiogram can be conducted. The imaging equipment and computer are syncronized with the patient's ECG, which identifies the temporal phases of the cardiac cycle. One cardiac cycle, represented by the R-R interval, is usually devided into 16 to 32 frames as shown in Figure 8.

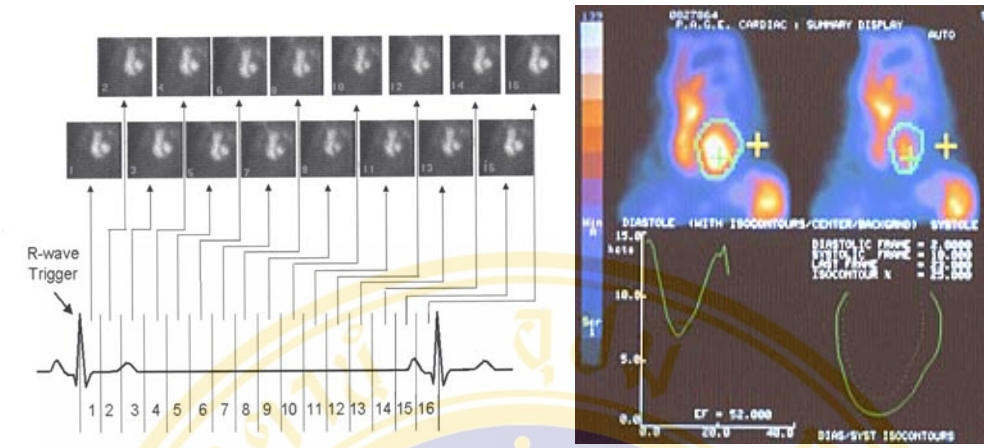

Figure 8. A, Diagram of gated data using 16 frames per R-R cardiac cycle (28). B, The count activities in the left ventricle are used to create a time/activity curve. These data can then be used to calculate ejection fraction values (29).

3.6.3 Gated SPECT Imaging

Early cardiac nuclear imaging studies were hampered by an inability to integrate myocardial perfusion imaging with studies of ventricular function. Since the development of gated SPECT in the late 1980s, this technique has been increasingly used for the assessment of the left ventricular function in the clinical setting and has now become routine part of SPECT equipment produced for myocardial perfusion imaging (30-32). Gated SPECT studies allow for the quantitative assessment of the LV function simultaneously with the evaluation of LV perfusion; accordingly, they provide powerful information for the risk assessment of patients with known or suspected coronary artery disease and aid in the assessment of myocardial viability. The most commonly radiopharmaceutical used in gated SPECT imaging is ^{99m}Tc-MIBI. When it is injected, it is taken up by the myocardium like myocardial perfusion studies.

- Image Acquisition

Gated SPECT imaging is a combination between a standard SPECT study and an equilibrium gated blood pool study. The difference between a standard SPECT and gated SPECT acquisition is that each view gated SPECT consists of 8

projection datasets (using 8 frames/cardiac cycle) instead of one dataset as received from a standard SPECT. Figure 9 compared the principle concept between a standard SPECT (Figure 9A) and gated SPECT acquisition (Figure 9B). For instance, for gated SPECT using 8 frames/cycle study and acquiring SPECT with 60 views/180 degree rotation, the number of projection is 480 images (8 frames x 60 views). To reformat from gated SPECT data into a standard SPECT data, each view or angle number of frames (8 frames) are summed into one image. As a result, the number of projections will be 60 as illustrated in Figure 10.

Before quantitative analysis, gated SPECT data are processed. All data in specific frames are added and images represent a specific phase of cardiac cycle. For example, for 8-frame study, the first frame of each view are summed together and so are the rest as illustrated in Figure 11. Finally there are 8 datasets and the 1st and 8th datasets are end-diastolic (ED) phase. Each dataset also consists of 60 views of projection data (SPECT data). Image reconstruction is performed for end-diastolic and end-systolic datasets. Afterward, LVEF will be estimated.

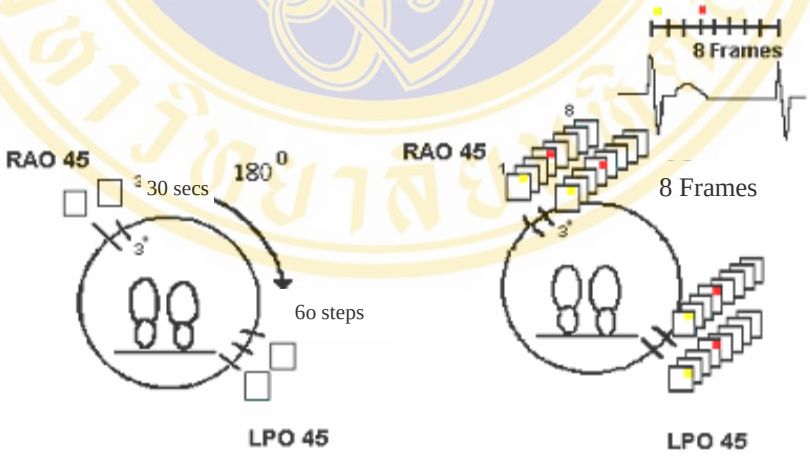

A. Standard SPECT **B. Gated SPECT**

Figure 9. A, In a standard SPECT study, for example a 180 degree, 60 steps, 30 sec/step setup, totally 60 projection images. B, In a gated SPECT study, 60 datasets have been acquired, with each data set composed of a set of 8 images, totally 480 images (33).

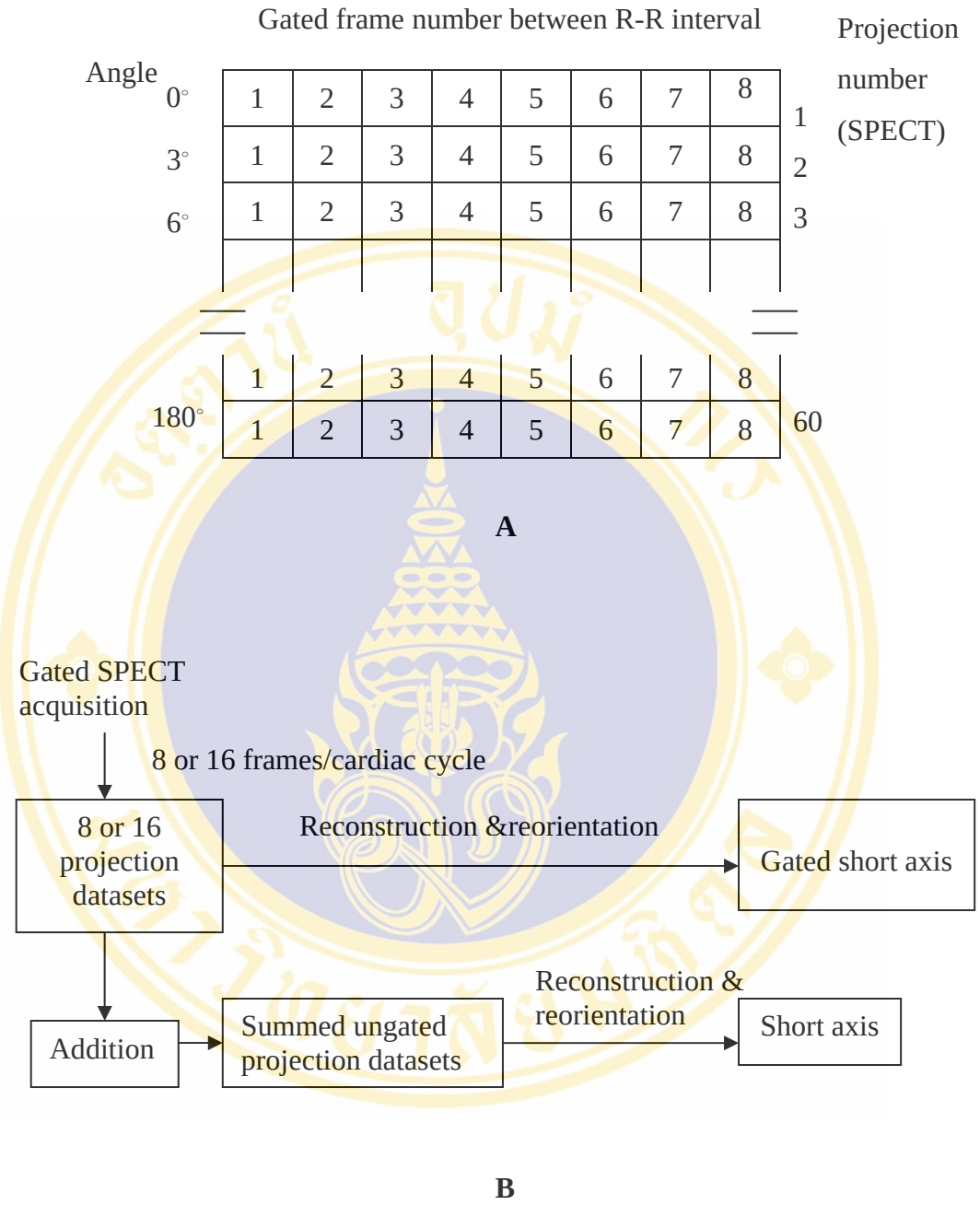

Figure 10. A, Illustration the gated SPECT acquisition, 8 projection images are acquired at each camera angle, 60 steps, totally 8x6 = 480 projection images. In the right hand, all frames are summed together for represented myocardial perfusion SPECT images. B, The general concepts of gated and ungated reconstruction.

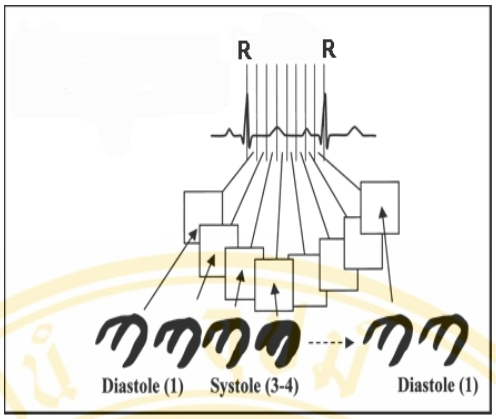

Figure 11. In gated SPECT acquisition, 1 cardiac cycle is divided into 8 frames, the 1st and 8th frames correspond to ED phase, while the 3rd or 4th frame correspond to ES phase (34).

3.6.4 Gated SPECT Analytic Methods

Gated SPECT images can be quantitatively analyzed with respect to a remarkable number of parameters of cardiac function, both global and regional. Global function is typically characterized by measurement of the left ventricular ejection fraction, which is the percentage of blood ejected from the left ventricle with each heart beat.

However, LVEF from gated SPECT can not be obtained directly as equilibrium gated blood pool. In equilibrium gated blood pool study, ventricular cavity counts are used to generate a time-activity curve, from which functional parameters are derived. But in gated SPECT study, the tracer is taken up by the left ventricular myocardium so that LVEF is derived from LV volume at end-diastole and end-systole. The end-diastolic volume and the end-systolic volume are identified as the largest and smallest LV cavity volume, respectively, and the %LVEF derived as (31)

$$\%LVEF = \frac{EDV - ESV}{EDV} \times 100 \qquad \text{.....(1)}$$

In this study, three gated SPECT software packages were used to quantitate data.

- Quantitative Gated SPECT (QGS) (35)

This algorithm is entirely automated to minimize the errors caused by inexperience users. The algorithm starts with:

1.) Segmentation of LV myocardium. The maximal voxel count value (C_{max}, likely corresponding to the myocardium) in the image volume is calculated. Left ventricle mask is generated using thresholding, clusterification and refined by eroding/dilating techniques. Then multiplying the mask by the original image isolates the left ventricle myocardium as shown in Figure 12.

Figure 12. A binary mask was generated from the original short-axis image volume (top two rows). Multiplying the mask by the original image isolates the left ventricular myocardium (bottom two rows) (35).

2.) Generation of myocardial surfaces (both endocardium and epicardium). The center of mass (COM) of LV is used as the origin coordinate system (should be located with LV cavity). Radial count profiles from COM are generated to achieve short-axis image volume. The locus of maximal count identifies the midmyocardial surface. Having found the midmyocardial surfaces for every interval, the geometry of end-diastolic surface is used to map the count distribution averaged over all intervals to determine the valve plane.

3.) A 25% threshold of those counts is taken and then fitted a plane. The valve plane in the end-diastole interval defines the myocardium as the collection of

surface points derived from the ellipsoidal sampling normals apical to the plane. The same normals are assumed to define the myocardium in all other intervals.

4.) For each interval, count profiles from midmyocardial surfaces are extracted. An asymmetric gaussian function is fitted to each profile. The Gaussians' maxima represent the midmyocardial surface, while the endocardial and epicardial surfaces are determined based on gaussian' s standard deviations.

5.) The endocardial volumes, EDV and ESV are used to calculate the global LVEF as in equation 1. Figure 13 presents a sample display of QGS.

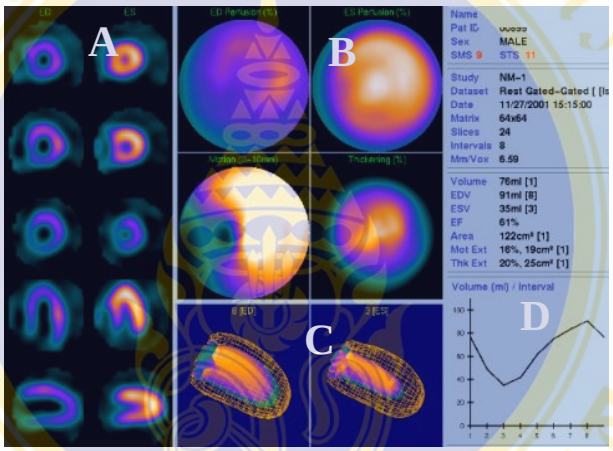

Figure 13. Quantification of ejection fraction, regional myocardial wall motion, and thickening from quantitative gated SPECT (QGS). A, Three short-axis (SA) images, a midventricular horizontal, and a midventricular vertical long-axis at end-diastolic (left column) and end-systolic (right column). B, Quantitative polar plots measuring regional myocardial wall perfusion, motion and wall thickening. C, Three-dimensional display of the endocardial (solid) and epicardial (grid) left ventricular surfaces calculated by the automatic algorithm. D, Endocardial time-volume curve and calculated LVEF from end-systolic and end-diastolic volumes.

- The Emory Cardiac Toolbox (ECTb)

The ECTb is developed at Emory University, Atlanta, GA by Faber et al (36). The principle of this algorithm is described below:

1.) The automatic processing begins by identifying the apex, base (valve plane) and the long-axis center of the LV, and a radius of search in which the myocardium can be entirely enclosed in every short-axis slice.

2.) A myocardial cylinder is defined by extending the detected myocardial circle (center and radius) through each slice of the short-axis volume. The maximal intensity of the volumetric image within the myocardial cylinder is determined.

3.) The base is considered to be the first slice basal to the center slice that does not contain a pixel greater than 65% of the maximum. The apex is considered to be the first slice apical to the center slice that does not contain a pixel greater than 40% of the maximum.

4.) The sampling is performed on the SPECT short-axis slices using a hybrid cylindrical-spherical coordinate system (Figure 14). Short-axis slices from the basal and medial portion of the LV were sampled using cylindrical coordinates, while the apical hemisphere was sampled using spherical coordinates.

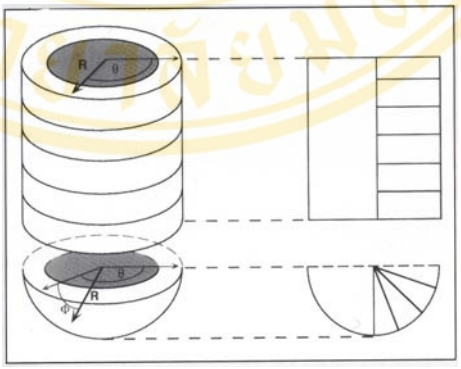

Figure 14. The coordinate system, the middle and basal portions of the LV are sampled using cylindrical coordinates, and the apical portion is sampled using spherical coordinates (37).

5.) By making an assumption based on MRI studies that the myocardium is approximately 10 mm thick at ED, the endocardial and epicardial boundary points could be estimated by subtracting and adding 5 mm on either of the midpoint of the myocardial wall, respectively. The modeling procedure is shown in Figure 15.

6.) Then the regional change in counts from the ED frame is used to determine the change in wall thickness and endocardial/epicardial surface locations at every frame in the cardiac cycle. For example if at ES the myocardial counts in a segment is double, the thickness will also be double from 10 to 20 mm.

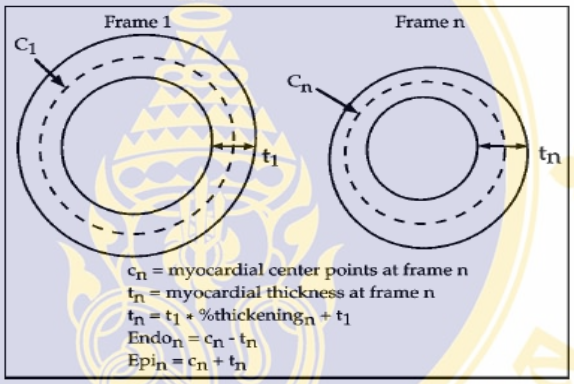

Figure 15. Demonstration of modeling technique used to define LV boundaries by the ECTb. At ED, myocardial wall thickness is assumed to be uniformly 10 mm thick (t_1). Percent thickening is used with base line value of 10 mm at ED to predict myocardial thickness at every additional frame in cardiac cycle. For every frame, half of myocardial thickness is added to myocardial center points to create epicardial surface points; half is subtracted to create endocardial surface points (36).

7.) In ECTb, the LV center, radial-search boundaries, and LV limits are identified as shown in Figure 16. Then the center and radius window displays eight short-axis slice images allowed the user review and modify the automatically selected LV center and radial boundaries for all eight gated frames as shown in Figure 17.

8.) Finally, the EDV and ESV is calculated to determine LVEF. A sample ECTb display is presented in Figure 18.

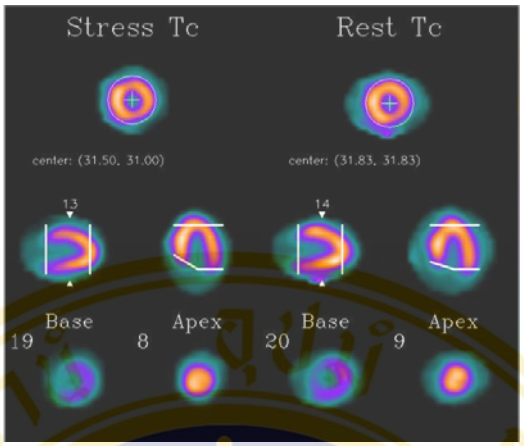

Figure 16. The top row shows midventricular short-axis slice images. These are used to illustrate the location of the radial search boundaries and LV center. The middle row shows both midventricluar vertical and horizontal long-axis reference images are used to illustrate the placement of the apical and basal slice selections. The bottom row displays short-axis slices, which correspond to the apical and basal slice selections identified in the middle row.

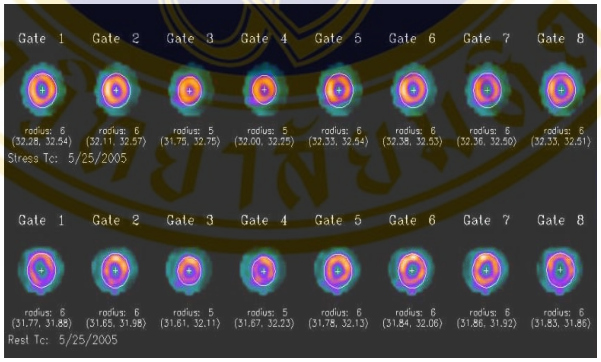

Figure 17. The LV center and radial boundaries are displayed for all gated frames.

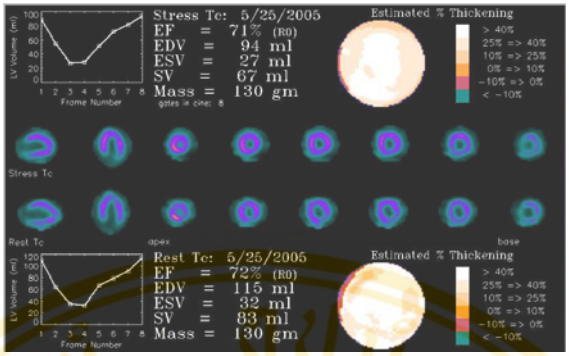

Figure 18. The volumes and ejection fraction (EF) window in ECTb provides LV volume curve and associated quantitative parameters.

- 4D-MSPECT (38)

This algorithm is semiautomated and it is a combination between QGS and ECTb. The program starts with:

1.) Finding the center of LV.

The center x_c and y_c are estimated by fitting an ellipse to the radial information from the circumferential profile analysis. For axial estimates (z_c, z-apical, z-basal), first, a linegram involving only the anterior portion of the mid axial slice down to the y_c estimate is used. The z-apical and z-basal are determine by taking a threshold of 55% of maximal activity of a linegrame. Then z_c is calculated by taking the integral midpoint between z-apical and z-basal.

2.) Finding LV surface.

Knowing the center and axial limits for the LV, long axis (LA) images are generated using bilinear interpolation from the SA volume. For this geometry, the program creates the sampling structure based on a cylindrical-spherical coordinate system. The cylindrical coordinate system is used to sample the LV from the basal to distal aspects. The spherical coordinate system is used to sample the apex. A gaussian fit is used to find the peak activity and an estimate of the myocardial thickness. The myocardial thickness at ED is scaled to be an average thickness of 10 mm. This scale factor in conjunction with a myocardial mass constraint is used to adjust the myocardial thickness throughout the cardiac cycle. Using the endocardial surfaces, a volume curve is generated and LVEF are computed. Figure 19 illustrates the display

for 4D-MSPECT software. Table 2 demonstrates the similarities and differences among QGS, ECTb and 4D-MSPECT.

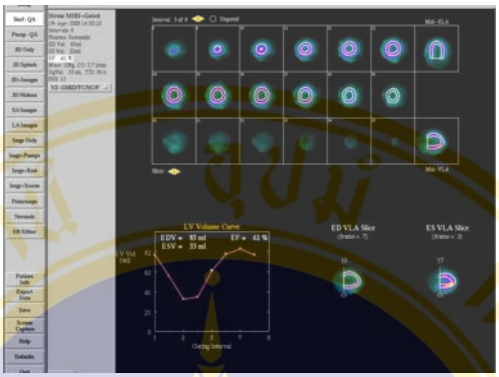

Figure 19. The image display window of the 4D-MSPECT contains: short-axis slices from apex to base, mid-ventricular horizontal and vertical long-axis with surface overlaid, the LV volume curve and LVEF. This screen allows the user to adjust the detected basal plane of the heart on the ED and ES vertical long-axis slices (two bottom right images).

Table 2. A comparison of features between QGS, ECTb and 4D-MSPECT.

	QGS	**ECTb**	**4D-MSPECT**
1. Processing	Automatic	Semi-automatic	Semi-automatic
2.Geometric model	Ellipsoid	- Cylindrical at base and LV medial portion - Spherical at apex	- Cylindrical at base and LV medial portion - Spherical at apex
3. Boundaries defined	Asymmetric gaussian fit	Count based method	Asymmetric gaussian fit
4. LV limits			
- apex	-	-< 40% of maximum counts	- 55% of maximum counts
- base	- 25% of maximum counts	-< 65% of maximum counts	- 55% of maximum counts

3.7 Image Reconstruction

In nuclear medicine, SPECT imaging is performed using a camera rotating around the patient and taking images of radioactive distribution within the patient from different angles. The image obtained each view is the projection of 3-dimensional (3D) distribution onto the 2-dimensional (2D) detector plane. To obtain a patient's image, the mathematical procedure to put the projections together called image reconstruction is performed (39,40). In general, there are two methods used in reconstructing images: analytical and iterative methods. Analytical methods are based on discrete implementations of analytical solutions of the inverse Radon transform problem. This method has a difficulty to incorporate models of image degradation factors such as collimator-detector response, attenuation and scatter. The most popular algorithm of the analytical reconstruction method is filtered backprojection (FBP). In nuclear medicine, iterative reconstruction has become popular for the following reason: (1) it is easy to model and handle image noise, especially when the counts are low; and (2) it is easy to incorporate with compensations of attenuation, collimator-detector response and scatter.

The basic principle of the iterative algorithms is to find a solution by successive estimates (Figure 20). The projections corresponding to the current estimate are compared with the measured projections. The result of the comparison is used to modify the current estimate, thereby creating a new estimate. When the projections of the current estimate are close to the measured projections, the correction factor is close to zero. The update and compare process is repeated until the difference between the estimated projections and measured projections falls below some specified level.

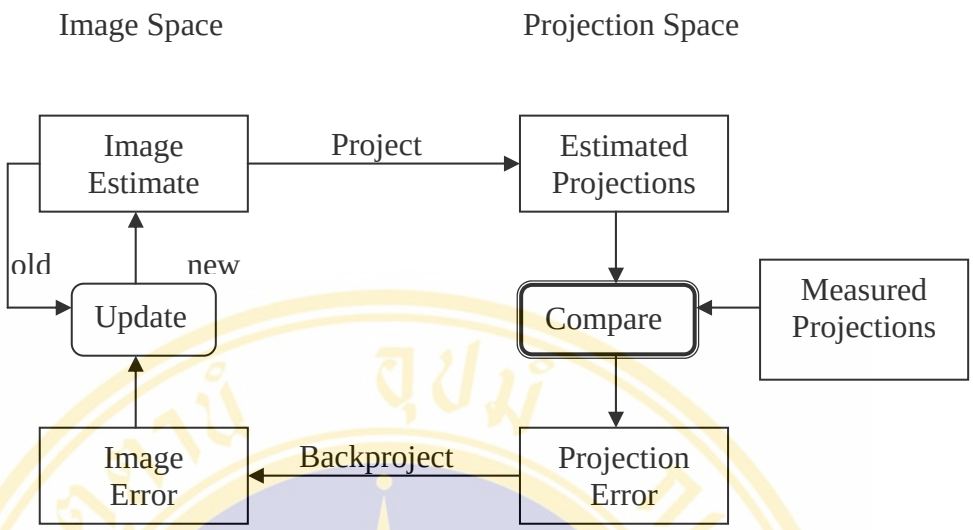

Figure 20. Schematic illustration of the steps in iterative reconstruction.

3.7.1 Filtered Backprojection (FBP)

The FBP is based on direct inversion of the Radon transform. This algorithm is fast and yields reliable quantitative results. However, for data with poor statistics, FBP results in poor image quality because of streak artifacts and low signal-to-noise ratio (SNR) (41). Figure 21 shows the image reconstruction process using a filtered backprojection algorithm. This algorithm involves the following steps:

1.) Compute the 1-D Fourier transform (FT) of a projection $(p(t,\phi))$.

2.) Multiply ($\otimes$) the FT of the projection ($P(\nu_t, \phi)$) by a filter function.

3.) Compute the inverse FT (FT^{-1}) of the filtered $p(\nu_t, \phi)$.

4.) Backproject to the image plane.

5.) Repeat steps 1-4 for all projections.

3.7.2 Ordered Subset Expectation Maximization (OS-EM)

The OS-EM has been proposed by Hudson and Larkin (43) to accelerate the reconstruction process using the maximum likelihood expectation maximization (ML-EM) algorithm. Since the OS-EM results from a simple modification of the ML-EM algorithm, an explanation of the OS-EM algorithm may be aided by starting from the formation of ML-EM. The ML-EM algorithm can be written as (44)

$$x_i^{new} = \frac{x_i^{old}}{\sum_j c_{ji}} \sum_j c_{ji} \frac{p_j}{\sum_k c_{jk} x_k^{old}} \qquad \text{.....(2)}$$

Where x_i represents the estimated intensity at pixel i and P_j represents the measured events in projection bin j. The c matrix, known as the transfer matrix, contains all the information about the imaging process such as attenuation, detector response, and scatter. That is modeled in the reconstruction. An element of the transfer matrix C, C_{ji}, represents the probability that a photon from pixel i will be detected in projection bin j. To obtain a new estimate of the image at pixel i, x_i^{new}, the old estimate, x_i^{old}, is multiplied by a correction factor. As shown in Equation 2, the correction factor is determined by computing the ratio between the measured projection, p and the current estimate projection, $\sum_k c_{jk} x_k^{old}$. This ratio for the pixel, $\sum_j c_{ji} \cdot p_j / \sum_k c_{jk} x_k^{old}$, is then backprojected, and normalized by $1/\sum_j c_{ji}$ and multiplied by x_i^{old}. The backprojection is performed for each projection bin.

The OS-EM algorithm maintains the same scheme as ML-EM with the difference the data are processed in subsets with each iteration. In the OS-EM algorithm, the estimated image is updated more frequently than in ML-EM. The formulation of this algorithm can be written as (45)

$$x_i^{new} = \frac{x_i^{old}}{\sum_{j \in S_n} c_{ji}} \sum_{j \in S_n} c_{ji} \frac{p_j}{\sum_k c_{jk} x_k^{old}} \qquad \text{.....(3)}$$

where S_n represents a subset of the projection bins j of the projection image p and the rest of the symbols have the same meaning as used in Equation 2. This algorithm groups the projection data into an ordered sequence of subsets. The projection errors, which are obtained from the difference between the measured and the estimated projections, are backprojected and used to generate the new estimate. The update continues until all the projection data have been processed. Then the process repeats again starting with the first subset. An iteration of OS-EM is completed when all the projection data have been used once in all the updates.

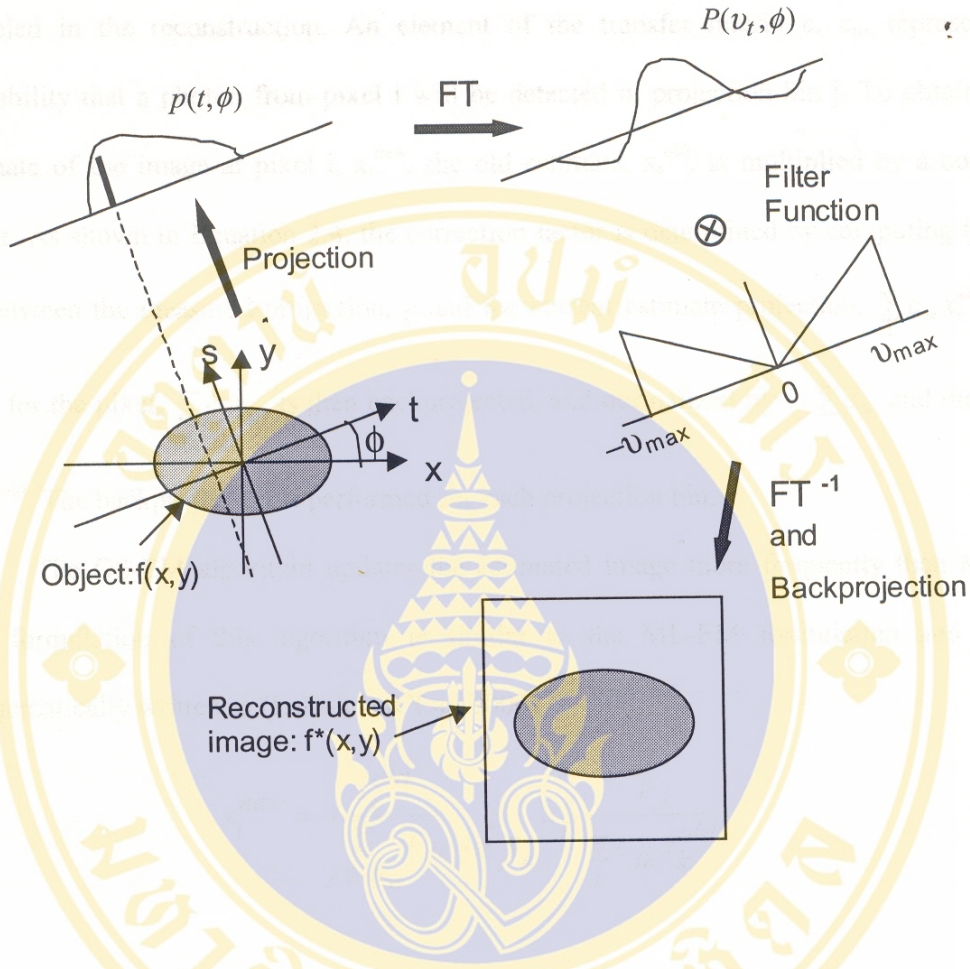

Figure 21. Image reconstruction using a filtered backprojection method. The projection data, p(t,ϕ) obtained from the object, f(x,y), are transformed into the frequency domain using FT. The FT of the projection data is multiplied by a filter function, and then the FT^{-1} of the filtered FT of the projection data is taken. The backprojection of the FT^{-1} projection data is performed. After repeating all the steps for all projections, the reconstructed image, f*(x,y), is obtained (42).

3.8 Literature Reviews

Regarding different results when using different algorithms of the same patient, there were few numbers of studies to compare the LVEF obtained from different algorithms. Vallejo et al. (46) evaluated the accuracy of QGS as a means of determining LVEF values that were compared with first-pass radionuclide angiography (FPRNA) in 400 patients. They found that LVEF from QGS is often lower than that from FPRAN. Accuracy was affected by high extracardiac activity, low count density, and small size of the left ventricle.

Gayed et al. (47) studied the effect of defect size and Tc-99m tetrofosmin dose on the accuracy of LVEF calculation using the automated QGS program. They reported that the LVEF obtained using high-dose (27 mCi) stress QGS correlated better with echocardiography than did that obtained using low-dose (8 mCi) rest QGS ($r = 0.86$ versus 0.76). Myocardial perfusion defects do not affect the accuracy of LVEF calculation using automated QGS.

Nichols et al. (2) compared QGS and ECTb for LVEF calculation in 246 patients who evaluated for CAD. The results of the comparison of the two software programs for calculated LVEF were found to correlate linearly ($r = 0.90$), but LVEF were significantly lower for QGS than with ECTb. Moreover, they studied in 50 healthy patients at low likelihood for CAD, for whom LVEF were significantly lower for QGS compared with ECTb.

Nakajima et al. (48) studied the accuracy of LVEF from 4 software programes; QGS, ECTb, 4D-MSPECT, and perfusion and functional analysis for gated SPECT (pFAST). Mathematic phantoms of cylindric-hemispheric hybrid models and clinical cases consisted of 30 patients who participated in a radionuclide angiography and gated blood pool (GBP) study in addition to undergoing ^{99m}Tc-MIBI gated SPECT were used. Patients were classified into 4 groups such as no defect, small defect, large defect, and small heart. They found that the LVEFs calculated from each software programs correlated well with the GBP study. The correlation coefficient between gated SPECT and the GBP study was 0.82, 0.78, 0.69 and 0.84 for QGS, ECTb, 4D-MSPECT, and pFAST, respectively. However, the LVEFs from QGS, ECTb, and 4D-MSPECT overestimated in patients with small hearts.

Due to several studies, LVEFs that calculated from gated SPECT have correlated well with gold standard, were accurate and reliable. However, this study used a different reconstruction algorithm. Therefore, the accuracy of LVEF from OS-EM reconstruction algorithm was evaluated.

CHAPTER IV
MATERIALS AND METHODS

4.1 Patient Population

This study was retrospective and seventy patients who were suspected of coronary artery diseases (CAD) and underwent myocardial gated SPECT imaging at the Section of Nuclear Medicine, Department of Radiology at Bumrungrad Hospital were used. All these patients were also performed echocardiography within one month. Forty-five patients were male and twenty-five patients were female and mean age was 62.69 ± 12.05 years (ranged from 19 to 89 years).

4.2 Image Acquisition and Reconstruction

4.2.1 Gated SPECT Acquisition

There were two image acquisition protocols used in this study. The first one was one-day protocol which the first dose of 8-10 mCi of ^{99m}Tc-sestamibi (^{99m}Tc-MIBI) was injected while the heart was at rest. The second dose of 24-30 mCi was injected during peak exercise and the interval between rest and stress studies was about three hours. The second one was two-day protocol which each injection dose was 24-30 mCi of ^{99m}Tc-MIBI. Since this study used stress study for LVEF calculation, the image acquisition and processing of stress study were described below.

Gated SPECT acquisition was performed using Siemens E.CAM dual head with a 90-degree configuration equipped with a low-energy high-resolution collimator (Figure 22). The projection data were acquired with 64x64 matrices, 32 views over 90 degrees for each detector at 30 secs per view. For gated mode, the cardiac cycle was divided into 8 frames/cycle.

Figure 22. SPECT Siemens E.CAM dual head in a 90-degree configuration.

4.2.2 Image Reconstruction

The projection data were reconstructed using iterative OS-EM algorithm. According to its properties , the image resolution is increased as the iteration number increases. However, image quality was degraded with the increment of image noise. As a result, the optimal number that compromises between resolution and noise should be first determined. We set up a pilot study to determine the optimal iteration number as follows. In order to make a fair comparison of left ventricular ejection fraction determination among three different software packages, the optimal number of iteration of each package was investigated. Thirty patients who were suspected of CAD and underwent both gated SPECT imaging and echocardiography were retrospectively studied. Each patient projection datasets were reconstructed using OS-EM algorithm with 8 angles/subset. No compensations for image degrading factors such as attenuation, detector response or scatter, were applied. Image reconstruction was performed with varying number of iteration from 1 to 6 reconstructed images were post-filtered with gaussian filter with 8 pixel-width. Then for each package, LVEF of each iteration number was determined using default setting to estimate left ventricular volume. Finally, the mean differences between echo and LVEF of each iteration number each package were calculated. The minimal mean difference was used as an optimal number. The results as reported in table 3 showed that the minimal mean differences between Echo and QGS, ECTb and 4D-MSPECT were 1.17, -2.00 and 0.10, respectively. Therefore, the optimal iteration numbers for QGS, ECTb and

4D-MSPECT were 3, 5 and 4, respectively. Those optimal iteration numbers were accordingly used in the rest of study.

4.3 Comparisons of The LVEF from Three Quantitative Gated SPECT Software Packages

4.3.1 The Effect of Apical and Basal Limits on The LVEF Calculation Using 4D-MSPECT

As mentioned before, LVEF was determined with estimation of LV volume from gated data. To define the edges of myocardium affects the volume calculation and ejection fraction afterward. All these three quantitative gated SPECT software packages such as QGS, ECTb and 4D-MSPECT have different methods to model the shape of the heart and volume. In image processing, QGS and ECTb use the automatic setting to define the volume of left ventricle while 4D-MSPECT is semiautomatic and users are allowed to modify the apical and basal limits. That might affect the accuracy of ejection fraction calculation due to different users. Therefore, in this session we studied the effect of the apical and basal limits on the LVEF calculation using 4D-MSPECT.

Projection datasets of gated data of 15 patients was used to study. Image reconstruction was performed using OS-EM with 8 angles/subset and 4 iterations and post-filtered with gaussian function at 8 pixel-width. LVEFs were determined with different apical and basal limits as follows:

1. At default settings or original position for both apical and basal limits as shown in Figure 23A and B.
2. At original position of basal limit, move apical setting one slice from original setting in and out at a time.
3. At original position of apical limit, move basal setting one slice from original setting in at a time twice, similarly more one slice out from original setting at a time for 2 slices.

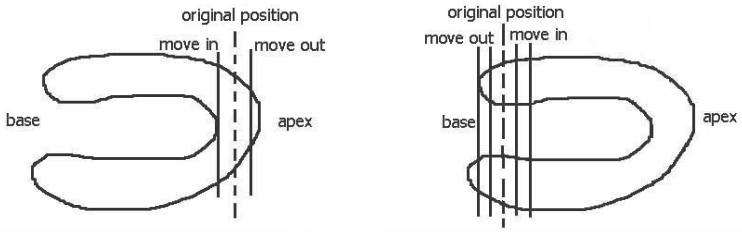

A **B**

Figure 23. A, The apical limit bars position. B, The basal limit bars position.

Table 4 showed that when moving the apical limit in or out 1 slice from the original position, the volume of left ventricle did not change. Whereas moving the basal limit in, the volumes gradually decreased and increased when moving the limit out. Therefore, users had to be cautions when positioning the limits especially on basal limits.

Table 3. The mean difference of LVEF from echocardiography compared with that from QGS, ECTb and 4D-MSPECT at 1st, 2nd, 3rd, 4th, 5th and 6th iterations.

Iteration No.	Mean Difference		
	Echo-QGS	Echo-ECTb	Echo-4D-MSPECT
1	-4.74	-11.67	-5.67
2	-1.27	-6.90	-2.57
3	**1.17**	-5.04	-1.14
4	2.33	-3.00	**0.10**
5	3.39	**-2.00**	0.83
6	4.23	-2.47	1.47

Table 4. The mean ± SD of LVEF values that calculated from 4D-MSPECT using original (automated) position, moved in and moved out one position to the center of LV of apical and basal limit bars, and moved in and moved out two position to the center of LV of basal limit bar.

Position	LVEF (%)	
	Apex	Base
Original	63.8±15.01	63.8±15.01
Move in 1 slice	63.8±15.04	61.3±15.54
Move in 2 slice	-	60.7±15.77
Move out 1 slice	63.8±15.01	64.0±15.10
Move out 2 slice	-	65.0±15.99

4.3.2 Accuracies of Determinations of LVEF from QGS, ECTb and 4D-MSPECT

This session was a study of the accuracies of LVEF determinations obtained from QGS, ECTb and 4D-MSPECT respectively compared with the LVEF obtained from echocardiography.

Seventy-patients were retrospectively studied. All patients underwent both gated SPECT imaging and echocardiography at Bumrungrad Hospital. Projection datasets of gated data were reconstructed using OS-EM algorithm with 8 angles/subset and at 3 iterations for QGS, 5 iterations for ECTb and 4 iterations for 4D-MSPECT respectively (data obtained from session 4.2)

4.3.2.1 Gated SPECT analysis

- QGS

1. Select patient file then projection data will be displayed as shown in Figure 24.
2. Select the area to be reconstructed.
3. Validate LV contours as shown in Figure 25.

4. Finally, the display as shown in Figure 26 will be pop up. The LVEF and bull's eye plot and LV at ED and ES are also included.

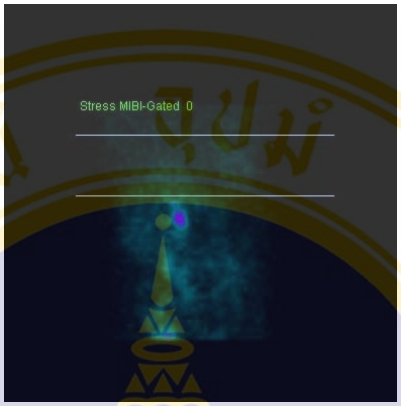

Figure 24. The projection data with reference lines.

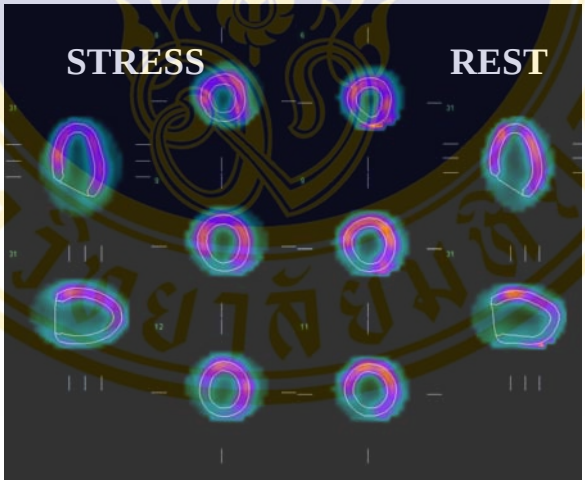

Figure 25. Myocardial contours overlaid by the automatically QGS algorithm.

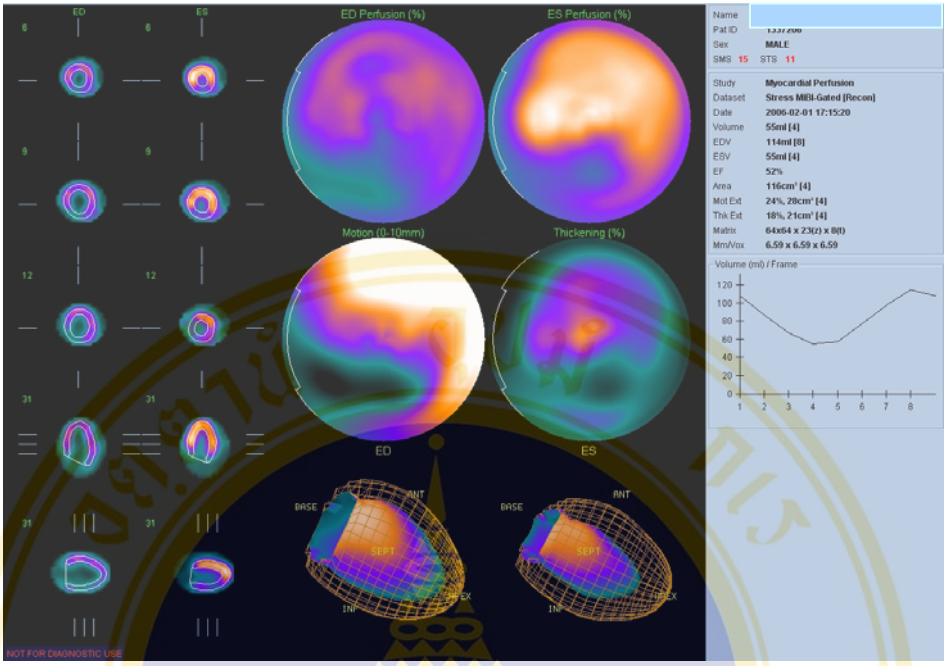

Figure 26. A sample display of QGS program.

- ECTb

1. Select the patient file.
2. Verify and change the automatically selected LV center and LV limits for both rest and stress images as shown in Figure 27.
3. Then choose “Function Analysis” to calculate LVEF.
4. Afterward, the LV center and radius as shown in Figure 28 are displayed.
5. The program allows user to verify apex and base as displayed in Figure 29.
6. Finally, The result of LVEF and bull’s eye plot are displayed in Figure 30.

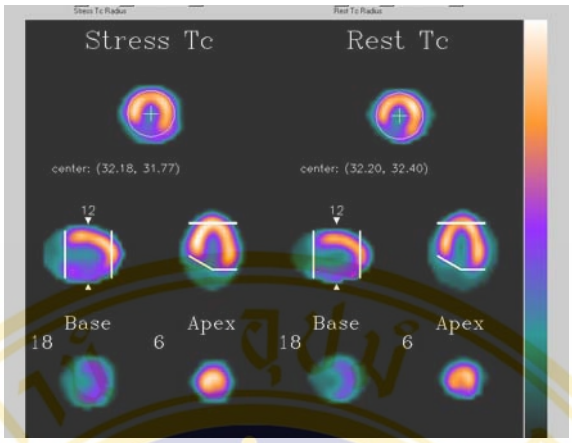

Figure 27. The locations of center, apex, and base are defined by default setting of ECTb program.

Figure 28. The center and radial boundaries are displayed for all 8 gated SPECT.

Figure 29. The apex and base locations are displayed.

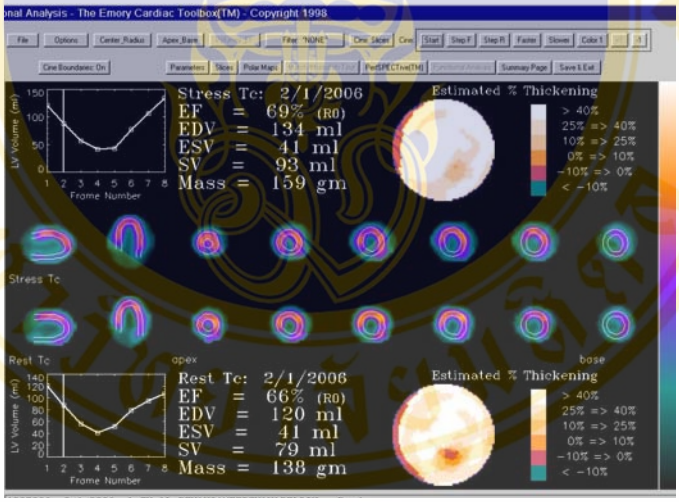

Figure 30. A sample display of ECTb program.

- 4D-MSPECT

1. Select the patient file and then 3 views of LV are displayed as shown in Figure 31.

2. The center of LV and the apical and basal limits are shown. At this step, users can change all the limits and center.

3. After defining the parameters, the LVEF is determined and displayed as shown in Figure 32.

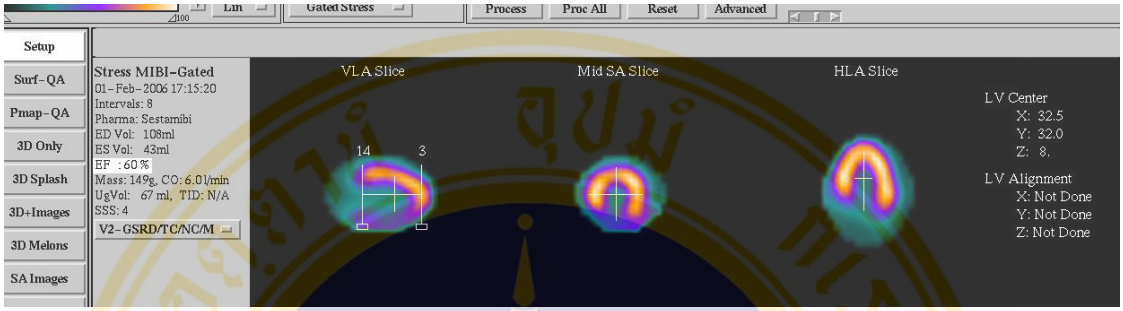

Figure 31. The center, apex, and base are displayed and the user can change for all parameters.

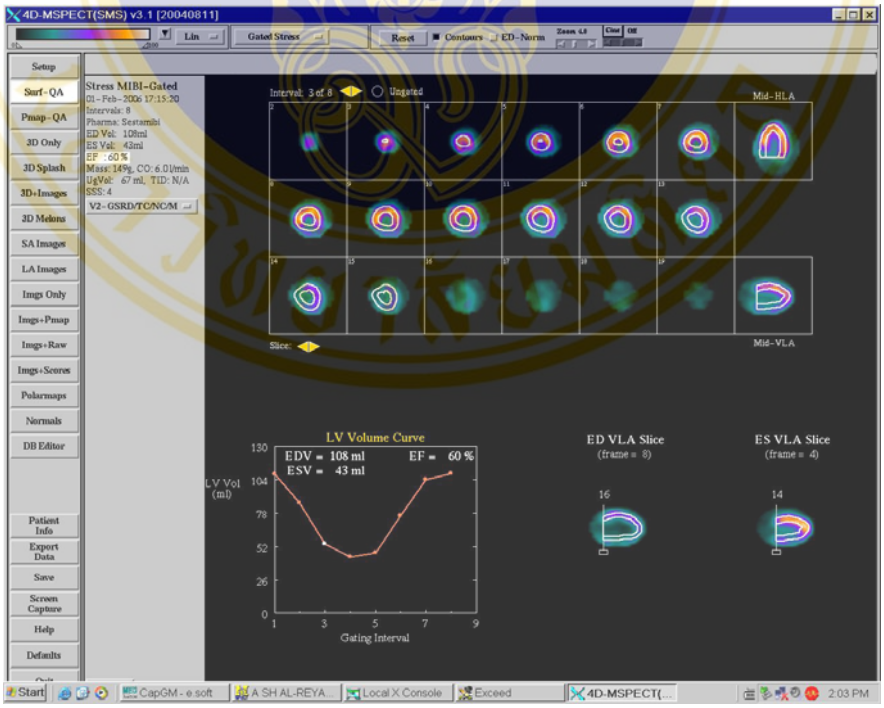

Figure 32. The sample display for 4D-MSPECT.

4.4 Comparison of The LVEF from Three Quantitative Gated SPECT Software Packages Using FBP with OS-EM Algorithm.

In nuclear cardiology, FBP algorithm is widely used in routine because of its speed and easy implementation. However, OS-EM algorithm has gained popularity because it provides good image quality especially when an image has low count. Moreover, image contrast can be improved using OS-EM algorithm. Hence, the volume of LV can be accurately calculated resulting in improving an accuracy of LVEF calculation. In this study, we compare LVEF calculated from FBP and OS-EM algorithms. The same projection datasets of seventy patients used in the previous session were reconstructed. No compensations for image degrading factors were applied. For FBP algorithm, reconstructed images were post-filtered with 5^{th} order Butterworth filter at 0.3 cycle/pixel cutoff frequency which is routinely used for myocardial SPECT at Bumrungrad Hospital. Then LVEFs were calculated using QGS, ECTb and 4D-MSPECT respectively. Finally, LVEFs obtained from FBP and OS-EM from each software package were compared.

4.5 Statistical Analysis

In this study, LVEF obtained from echocardiography was used as a gold standard. Then the difference between LVEFs from echo and each package was calculated. Those differences were averaged and the standard deviation was computed. A two–tailed pair t-test was used to test for statistical significance of the mean of the difference for each pair. The critical value, t, is defined as (49)

$$t = \frac{\sqrt{n}D_{ave}}{SD} \qquad \text{.....(4)}$$

Where D_{ave} is the average difference of pairs in the LVEF of each pair data, SD is the standard deviation of the difference and n is the number of data. If p-value obtained from the t value for n-1 degree of freedom was less than 0.05, that meant there was a statistically significant difference between the LVEF of each pair data. Moreover, QGS and ECTb, QGS and 4D-MSPECT, and ECTb and 4D-MSPECT were studied using linear regression analysis. It is computed from (49)

$$y = a + bx \quad \text{……(5)}$$

Where y is estimated LVEF when given x (measured LVEF). The parameter a is y-axis intercept and b is the slope, $\Delta y/\Delta x$. Finally, correlation coefficient, r, is computed from (49)

$$r = b(SD_x / SD_y) \quad \text{...……(6)}$$

Where *SD* is the standard deviation. The value of r is such that $-1 \leq r \leq +1$. If x and y have a strong positive linear correlation, r is close to +1. It means that a relationship between x and y variables such that as values for x increases, values for y also increase. If x and y have a strong negative linear correlation, r is close to -1. It means that a relationship between x and y variables such that as values for x increases, values for y decrease. If there is no linear correlation or a weak linear correlation, r is close to 0. A value near zero means that there is a random, nonlinear relationship between the two variables.

In the study of %LVEFs obtained from OS-EM and FBP, a pair t-test was also used to test the statistical significance in mean difference between %LVEF from those two reconstructed algorithms. If p-value was less than 0.05, that meant there was statistically significant difference in %LVEF. The linear regression was also used to test the correlation between %LVEFs from OS-EM and FBP in each software package.

CHAPTER V
RESULTS

5.1 Comparisons of the LVEF from Three Quantitative Gated SPECT Software Packages.

The ejection fractions calculated by echocardiography, QGS, ECTb, and 4D-MSPECT for the 70 patients who were suspected of CAD were shown in Table 5 and the mean values of LVEF were shown in Table 6. The results showed that the mean LVEFs were 61.75% ± 13.69% for echocardiography, 60.43% ± 16.23% for QGS, 63.74% ± 15.27% for ECTb, and 61.91% ± 15.12% for 4D-MSPECT. Using echocardiography as a gold standard, Table 7 revealed that on average LVEF from QGS was 1.32 less than that from echocardiography but this difference was not statistically significant ($p = 0.259$). In terms of 95% confidence interval (CI) of the difference, if the mean of the difference in LVEF between echocardiography and QGS was between -0.99 and 3.64. That means there is no statistically difference with 95% CI. Figure 33 showed the scatter plot between %LVEFs from echocardiography and QGS. The plot showed that %LVEFs from QGS were most likely less than that from echocardiography. For a pair of echocardiography and ECTb, the average difference was -1.99. That means the average LVEF from ECTb was 1.99 more than that from echocardiography. The difference was not statistically significant with p-value = 0.051 and the 95% CI of the difference in LVEF was between -3.99 and 0.01. Therefore, the average difference in LVEF between echocardiography and ECTb was not statistically significant with 95% CI. Figure 34 showed a scatter plot between %LVEFs from echocardiography and ECTb. The plot showed that %LVEFs from ECTb were most likely higher than that from echocardiography, that agreed with the statement above. Table 7 also showed that the average difference of LVEF obtained from 4D-MSPECT was 0.16 more than echocardiography and the difference was not statistically significant with p-value = 0.861. Figure 35 demonstrated a scatter plot between %LVEFs from echocardiography and 4D-MSPECT and it showed that

%LVEFs from 4D-MSPECT were slightly more than that from echocardiography. In term of 95% CI, the difference of LVEF was between -2.04 and 1.71; therefore, the average difference in LVEF between echocardiography and 4D-MSPECT was not statistically significant with 95% CI. The average differences and 95% CI of each pair data were graphically plotted as shown in Figure 36. If the 95% CI value crossed zero-line that meant the difference was not statistically different.

Figure 37 showed the correlation between the %LVEFs of QGS and ECTb. The plot revealed that the correlation between QGS and ECTb was high (r = 0.95) and the slope of the regression line was 1.005. Figure 38 also showed correlation between the %LVEFs of QGS and 4D-MSPECT. It showed that the correlation was high (r = 0.95) and the slope of the regression line was 1.015. The correlation between the %LVEFs of 4D-MSPECT and ECTb was shown in Figure 39. It demonstrated that the correlation was high (r = 0.96) and the slope of the regression line was 0.95.

Table 5. The LVEFs that obtained from echocardiography, QGS, ECTb and 4D-MSPECT.

No.	LVEF (%)				No.	LVEF (%)			
	Echo	QGS	ECTb	4D-M		Echo	QGS	ECTb	4D-M
1	52.19	45	52	54	**36**	57.51	56	65	57
2	78.58	60	71	72	**37**	62.73	62	61	64
3	71.72	74	81	76	**38**	60.91	83	84	78
4	76.41	62	70	62	**39**	40.89	20	28	25
5	57.83	50	62	65	**40**	62.68	54	64	61
6	74.76	73	68	72	**41**	48.63	40	37	50
7	67.68	79	80	77	**42**	65.37	49	56	49
8	35.34	32	31	30	**43**	43.48	40	44	39
9	56.17	54	56	59	**44**	66.64	49	53	48
10	60.28	52	59	52	**45**	80.92	74	75	75
11	75.02	60	66	67	**46**	28.76	39	42	39
12	76.73	88	88	89	**47**	52.13	44	59	47
13	32.37	36	41	32	**48**	73.64	65	77	78
14	67.85	80	71	71	**49**	69.13	55	61	62
15	73.46	64	59	60	**50**	43.4	46	39	41
16	53.92	47	50	52	**51**	73.27	75	79	78
17	57.34	64	69	62	**52**	65.03	69	66	65
18	75.56	78	86	77	**53**	65.09	60	73	68
19	31.31	53	52	45	**54**	59.84	65	68	69
20	24.90	26	38	29	**55**	65.57	73	67	70
21	62.2	62	65	64	**56**	78.43	73	78	78
22	64.67	73	67	67	**57**	72.39	73	74	74
23	72.03	78	80	70	**58**	72.54	58	61	59
24	51.31	52	51	53	**59**	73.91	63	70	75
25	26.74	20	22	29	**60**	79.36	86	85	79
26	68.87	85	86	84	**61**	64.25	60	61	60
27	53.15	39	46	42	**62**	69.22	69	70	69
28	73.85	66	65	65	**63**	53.12	53	55	56
29	67.47	62	65	62	**64**	70.04	76	80	80
30	71.24	62	74	69	**65**	65.00	77	75	73
31	72.70	76	75	71	**66**	53.77	54	55	55
32	70.42	85	83	79	**67**	68.30	65	71	70
33	62.97	57	71	68	**68**	64.52	83	82	83
34	59.16	48	55	48	**69**	38.08	34	38	38
35	64.20	61	68	65	**70**	73.54	85	86	83

Table 6. Comparison of mean ± SD of LVEFs obtained from echocardiography, QGS, ECTb, and 4D-MSPECT.

	Mean	SD	Min, Max
Echocardiography	61.75	13.69	24.9, 80.92
QGS	60.43	16.23	20, 88
ECTb	63.74	15.27	22, 88
4D-MSPECT	61.91	15.12	25, 89

Table 7. Comparison of mean difference of LVEF obtained from echocardiography, QGS, ECTb and 4D-MSPECT.

	Echo - QGS	Echo - ECTb	Echo - 4D-MSPECT
Mean ± SD	1.32 ± 9.72	-1.99 ± 8.39	-0.16 ± 7.85
(Min, Max)	-22.09, 20.89	-23.09, 14.46	-18.48, 18.64
p-value	0.259	0.051	0.861
95% CI	-0.99, 3.64	-3.99, 0.01	-2.04, 1.71

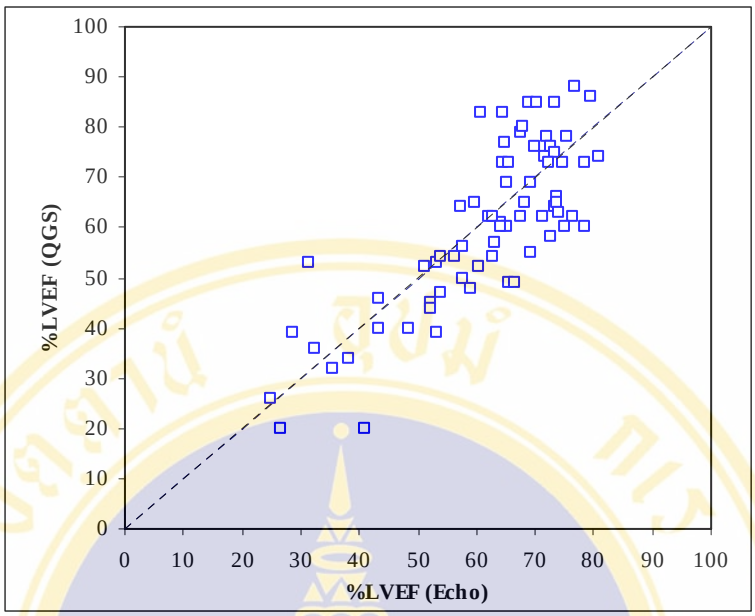

Figure 33. The scatter plot between % LVEF from echocardiography and QGS.

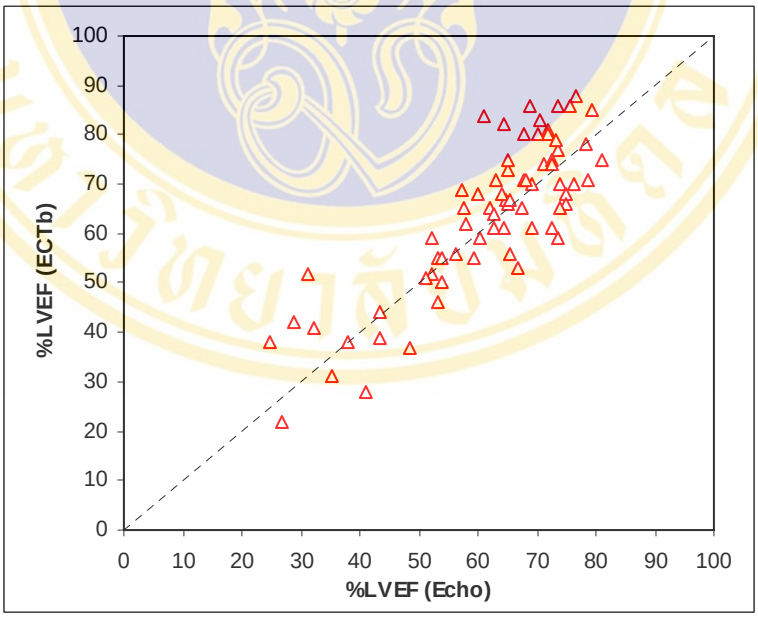

Figure 34. The scatter plot between %LVEF from echocardiography and ECTb.

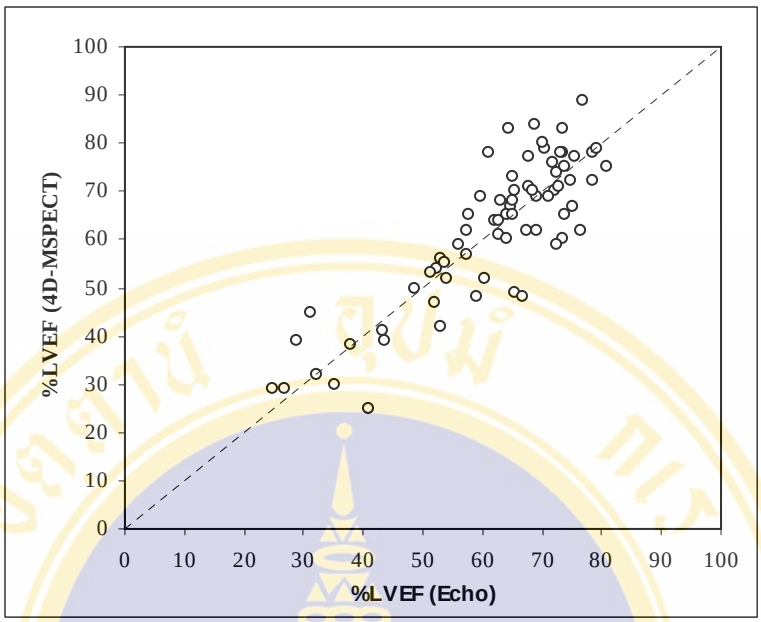

Figure 35. The scatter plot between %LVEF from echocardiography and 4D-MSPECT.

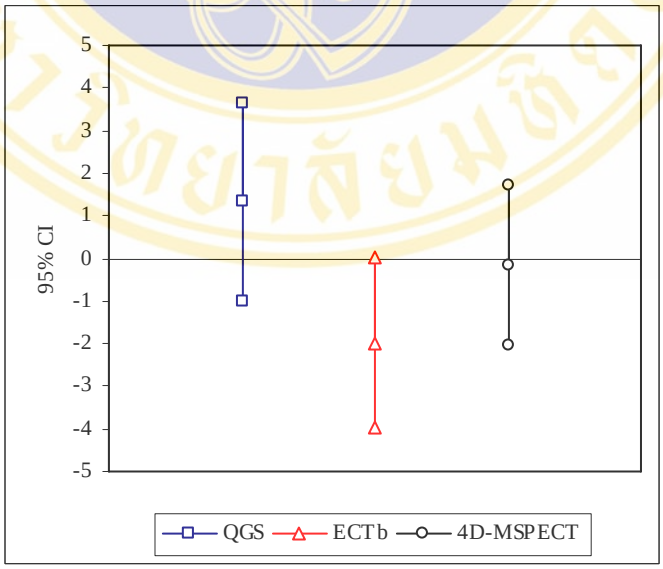

Figure 36. The average differences and 95% CI between echocardiography and three quantitative gated SPECT software packages.

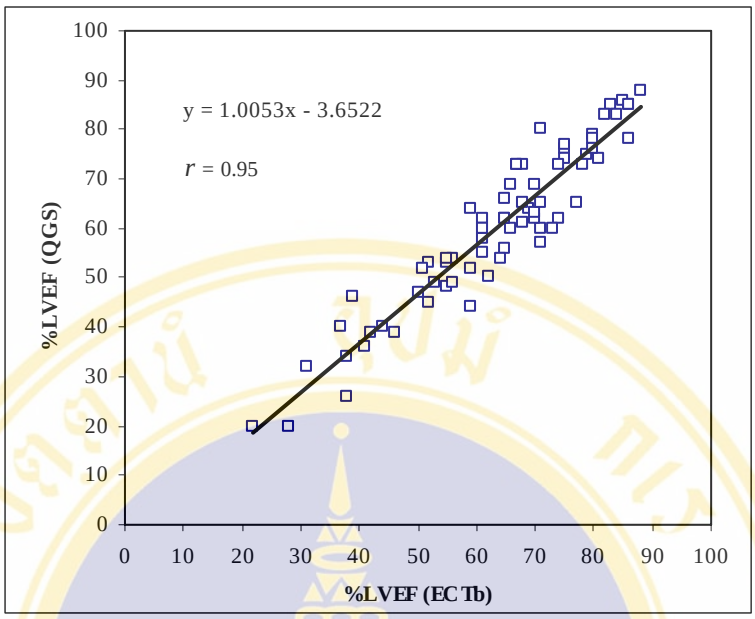

Figure 37. The correlation analysis of %LVEFs estimated from QGS and ECTb.

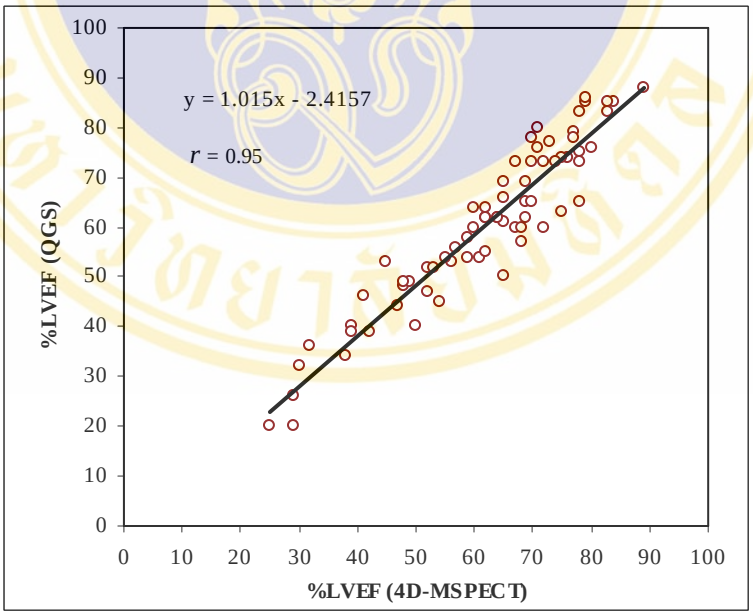

Figure 38. The correlation analysis of %LVEFs estimated from QGS and 4D-MSPECT.

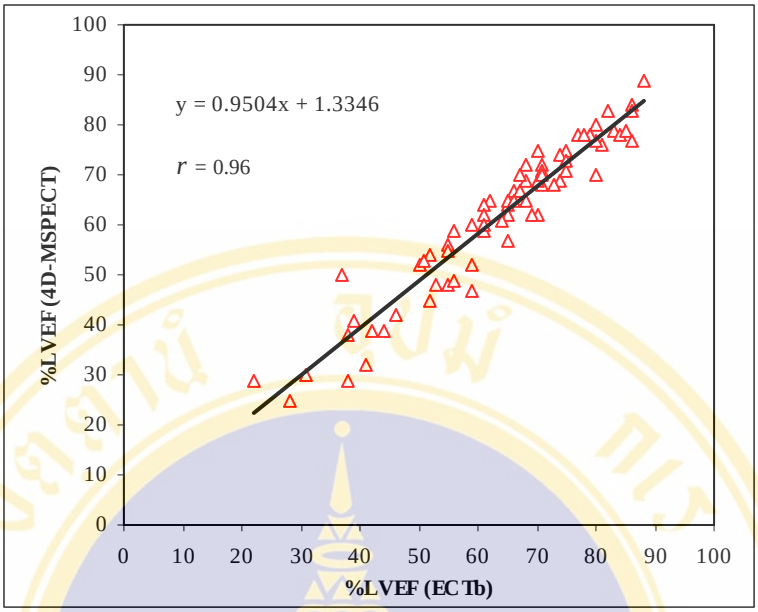

Figure 39. The correlation analysis of %LVEFs estimated from 4D-MSPECT and ECTb.

5.2 Comparison of The LVEF from Three Quantitative Gated SPECT Software Packages Using FBP with OS-EM Algorithm.

The percentages of LVEF obtained from OS-EM and FBP reconstructed algorithms were determined. Table 8 reported the mean difference, standard deviation and p-value in each package. The results showed that there were no significantly different in %LVEF between OS-EM and FBP for QGS and 4D-MSPECT software packages with p-value > 0.05. For ECTb, the result showed that the difference was statistically significant with p-value < 0.001.

The correlation between the %LVEFs of QGS using FBP and OS-EM algorithm was shown in Figure 40. It showed that the correlation between using FBP and OS-EM algorithm was high (r = 0.98). The slope of the regression line was 0.99. Figure 41 showed the correlation between the %LVEFs of ECTb using FBP and OS-EM algorithm. It also showed that the correlation was high (r = 0.96). The slope of the regression line was 1.02. Figure 42 showed the correlation between the %LVEFs of 4D-MSPECT using FBP and OS-EM algorithm. It demonstrated that the correlation was likewise high (r = 0.96). The slope of the regression line was 1.08.

Table 8. Mean differences and standard deviations of %LVEF obtained from OS-EM and FBP for each software package.

	OS-EM - FBP		
	QGS	**ECTb**	**4D-MSPECT**
Mean ± SD	0.69 ± 2.96	-2.16 ± 4.68	-1.00 ± 4.68
(Min, Max)	-12, 6	-15, 9	-22, 9
p-value	0.057	<0.001	0.078
95% CI	-0.02, 1.39	-3.27, -1.04	-2.12, 0.12

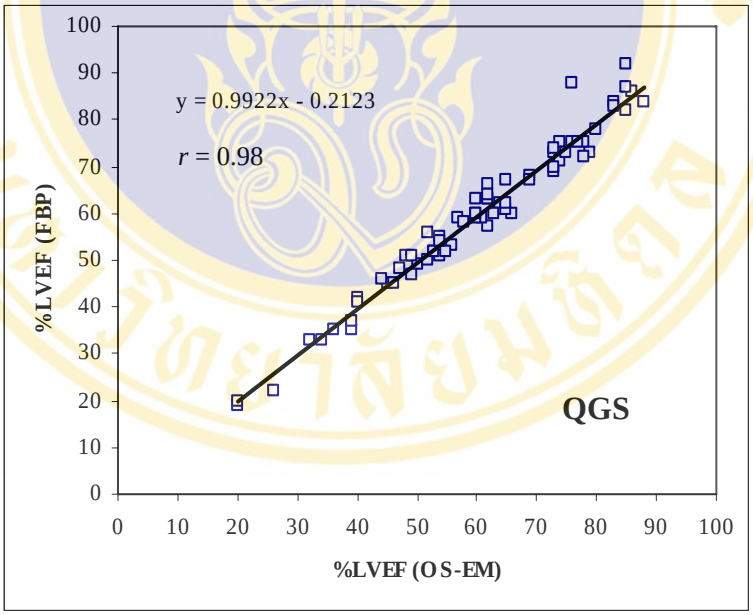

Figure 40. The correlation analysis of %LVEFs estimated from QGS using FBP and OS-EM algorithm.

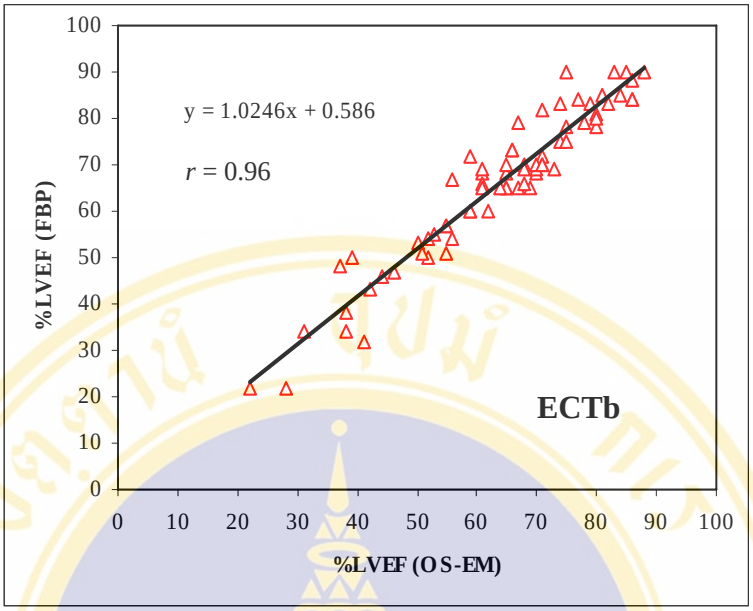

Figure 41. The correlation analysis of %LVEFs estimated from ECTb using FBP and OS-EM algorithm.

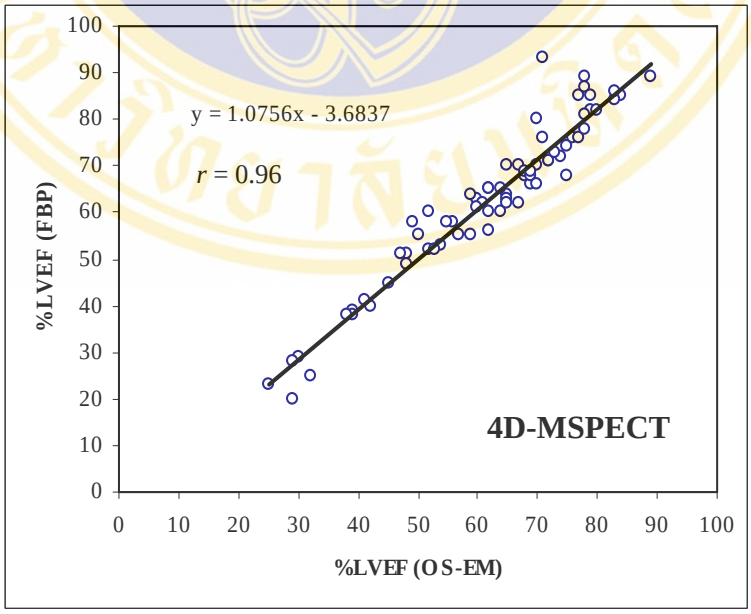

Figure 42. The correlation analysis of %LVEFs estimated from 4D-MSPECT using FBP and OS-EM algorithm.

CHAPTER VI
DISCUSSION

6.1 Comparisons of The LVEF from Three Quantitative Gated SPECT Software Packages.

In this study, we investigated the accuracy of LVEFs calculated from QGS, ECTb, and 4D-MSPECT in seventy patients and using LVEF from echocardiography as a gold standard. Echocardiography was used as the method of reference in this study because at Bumrungrad Hospital, it is a screening investigation for patients who were suspected for CAD. We found that there were no statistically significances in mean differences of LVEF between echocardiography and all three software packages. However, the LVEF from QGS most likely underestimated than that from echocardiography, while the LVEF from ECTb most likely overestimated. For 4D-MSPECT, LVEF was slightly different from that calculated from echocardiography. Our findings have similarity and differences from other studies as follows. Nakajima et al. (48) compared LVEFs from QGS, ECTb, 4D-MSPECT and pFAST (Sapporo Medical University, Sapporo, Japan) with that from gated blood pool (GBP) study in 30 patients. They found that LVEFs estimated from ECTb and 4D-MSPECT were slightly higher than that found by the GBP study. For patients with small hearts; QGS, ECTb, and 4D-MSPECT gave the overestimated LVEF. This result agreed with Vallejo et al. (50) who studied the LVEFs in canine. They found that the LVEFs calculated from QGS were significantly greater than cardiac MRI (cMRI). This is most likely because dog hearts, on average, are much smaller than human hearts, and SPECT techniques are known to overestimate LVEFs in very small hearts, due to partial volume effect.

Schaefer et al. (51) studied the accuracy of QGS, ECTb, and 4D-MSPECT in assessment of LVEFs using cMRI as a reference. They found that LVEFs calculated from ECTb and 4D-MSPECT did not differ significantly from cMRI, whereas QGS

values were significantly lower than cMRI. Faber et al. (52) reported that LVEFs measured from ECTb are not significantly different from cMRI but from QGS significantly underestimated the cMRI values. Vallejo et al. (46) showed that mean LVEF from QGS was lower than from first-pass radionuclide angiography (FPRNA).

We also studied the correlation between each pair of software packages (QGS vs ECTb, QGS vs 4D-MSPECT, and 4D-MSPECT vs ECTb) using linear regression analysis. All correlation coefficients were high, with values greater than 0.9. It is probably more meaningful to ask which gated SPECT methods correlated well with one another. In this sense, it is possible to predict one method's results from the results of another for LVEFs. These are agreed with Lum and Coel (53) who reported those methods correlated well with one another. For QGS and ECTb, Nichols et al. (4, 2) found that the correlation coefficients between two methods were high. Furthermore, they reported that LVEFs were significantly lower for QGS compared with ECTb.

6.2 Comparison of The LVEF from Three Quantitative Gated SPECT Software Packages Using FBP with OS-EM Algorithm.

FBP algorithm has been the most widely used for myocardial SPECT reconstruction for a decade. Recently, OS-EM has now become an alternative algorithm because it provides a better image quality such as contrast, signal to noise ratio, and resolution (54). As we discussed previously, the LVEFs estimated from gated SPECT were derived from left ventricular volume and the edge detection and volume calculation obtained from OS-EM might be more accurate. Therefore, the LVEFs from OS-EM and each software package were compared to that from FBP.

We found that there were no statistically significance in %LVEF between those two algorithms for QGS and 4D-MSPECT software packages with $p > 0.05$. While for ECTb software package, there was statistically significant difference with $p < 0.05$. The correlation between those two algorithms for each software package was high with $r > 0.9$. That meant the %LVEF from OS-EM was reliable and can be used as a substitute to that from FBP.

6.3 Clinical Relevance of the Study.

Although the sample size of this study might not sufficiently large to demonstrate the statistically significance, our results revealed the characteristic of each package. That leads to the cautions for data interpretation. Yet, our study showed that the LVEFs from those three software packages were interchangable. That helped users for follow-up cases when upgrading systems or softwares. Similarly, the LVEFs from OS-EM algorithm were also reliable and can be interchanged with that from FBP.

REFERENCES

1. Cwajg E, Cwajg J, He Z, Hwang WS, Keng F, Nagueh SF, et al. Gated myocardial perfusion tomography for the assessment of left ventricular function and volumes: comparison with echocardiography. J Nucl Med.1999; 40:1857-65.
2. Nichols K, Santana CA, Folks R, Krawczynska E, Cooke D, Faber TL, et al. Comparison between ECTb and QGS for assessment of left ventricular function from gated myocardial perfusion SPECT. J Nucl Cardiol 2002; 9:285-93.
3. Garcia EV, Santana C, Faber TL, Cooke D. Methods for evaluating left ventricular function computed from ECG-gated myocardial perfusion SPECT. 2nd virtual congress of cardiology. [online] date unknown [cited 2005 Dec 17] Available from: URL: http://www.fac.org.ar/scvc/llave/image/garcia/garciai.htm
4. Nichols K, Lefkowitz D, Faber T, Folks R, Cooke D, Garcia EV, et al. Echocardiographic validation of gated SPECT ventricular function measurements. J Nucl Med.2000;41:1308-14.
5. Nichols K, DePuey EG, Rozanski A. Automation of gated tomographic left ventricular ejection fraction. J Nucl Cardiol. 1996;3:475-82.
6. Vaduganathan P, He ZX, Vick CW, Mahmarian JJ, Verani MS. Evaluation of left ventricular wall motion, volumes, and ejection fraction by gated myocardial tomography with technetium 99m-labeled tetrofosmin: a comparison with cine magnetic resonance imaging. J Nucl Cardiol.1999;6:3-10.
7. Lipke CS, Kuhl HP, Nowak B, Kaiser H, Reinartz P, Koch K. Validation of 4D-MSPECT and QGS for quantification of left ventricular volumes and ejection fraction from gated ^{99m}Tc-MIBI SPET: comparison with cardiac magnetic resonance imaging. Eur J Nucl Med Mol Imaging 2004;31:482-90.
8. Boellaard R, Lingen A, Lammertsma AA. Experimental and clinical evaluation of iterative reconstruction (OSEM) in dynamic PET: quantitative characteristics and effects on kinetic modeling. J Nucl Med 2001;42:808-17.

9. Gutman F, Gardin I, Delahaye N, Rakotonirina H, Hitzel A, Manrique A. Optimaisation of the OS-EM algorithm and comparison with FBP for image reconstruction on a dual-head camera: a phantom and a clinical ^{18}F-FDG study. Eur J Nucl Med Mol Imaging 2003;30:1510-19.
10. Bettinardi V, Pagani E, Gilardi M, Alenius S, Thielemans K, Teras M, et al. Implementation and evaluation of a 3D one-step late reconstruction algorithm for 3D positron emission tomography brain studies using median root prior. Eur J Nucl Med 2002; 29:7-18.
11. Kaufman R. Coronary artery disease (CAD). Teaching Affiliate [online] 2003 November [cited 2006 Feb 1];[4 screens]. Available from: URL: http://healthgate.partners.org/browsing/BrowseContent.asp?fileName=11986.xml&title=Coronary%20Artery%20Disease%20(CAD)
12. Coronary heart disease [homepage on the Internet].date unknown [cited 2006 Feb 7];[1 screen]. Available from: URL: http://www.answers.com/topic/coronary-heart-disease.
13. Nissl J, Payne K. Electrocardiogram. A-Z health guides [online] 2004 April [cited 2006 Feb 8];[1 screen]. Available from: URL: http://www.webmd.com/hw/heart_disease/hw213248.asp
14. Coronary artery disease [homepage on the Internet] 2005 August [cited 2006 Feb 8]; [1 screen]. Available from: URL: http://www.cnn.com/HEALTH/library/DS/00064.html
15. Electrocardiogram. [homepage on the Internet] date unknown [cited 2006 Feb 8]. Available from: URL: http://yalenewhavenhealth.org/library/healthguide/en-us/support/topic.asp?hwid=zm2351
16. Echocardiogram[homepage on the Internet] date unknown [cited 2006 Feb 8]. Available from: URL: http://www.chicagoheart.com/tee.htm
17. Cardiac catheterization [homepage on the Internet] date unknown [cited 2006 Feb 10]. Available from: URL: http://www.chh.org/?tabId=22
18. Cardiovascular MRI [homepage on the Internet] date unknown [cited 2006 Feb 10]. Available from: URL: http://www.lifespan.org/Services/DiagImag/MRI_Ctr/cardiac/mri2.jpg

19. Broderick LS. Computed tomography of the heart and pericardium. In: Haaga JR, Lanzieri CF, Gilkeson RC, editors. CT and MRI imaging of the whole body. 4th ed. St. Louis: Mosby; 2003.p.1063-88.

20. Chan FP. Cardiac MDCT. In: Fishman EK, Jeffrey RB, editors. Multidetector CT: principles, techniques, and clinical applications. Philadelphia: Lippincott Williams & Wilkins; 2004.p.129-58.

21. Screenshots [homepage on the Internet] date unknown [cited 2006 Feb 20]. Available from: URL: http://homepage.mac.com/rossetantoine/osirix/Snapshots.html

22. Thrall JH, Ziessman HA. Cardiovascular system. In: Thrall JH, editor. Nuclear medicine. 2nd ed. St. Louis: Mosby; 2001.p.65-109.

23. Iskandrian AS, Verani MS. Instrumentation and technical considerations in planar and SPECT imaging. In: Iskandrian AS, Verani MS, editors. Nuclear cardiac imaging: principles and applications. 2nd ed. Philadelphia: F.A.Davis; 1996. p.29-45.

24. Larock M-P, Braat SH, Sochor H, Maisey M, Rigo P. Myocardial imaging: technetium ^{99m}Tc sestamibi. London: Martin Dunitz; 1993. p. 1-16.

25. Germano G. Technical aspects of myocardial SPECT imaging. J Nucl Med. 2001; 42: 1499-1507.

26. Atlas of myocardial perfusion SPECT [homepage on the Internet] 1999 April [cited 2006 Jan 25]. Available from: URL: http://www.brighamrad.hardvard.edu/education/online/cardiac/Gated-SPECT.html.

27. Hauser TH, Danias PG. Indications for equilibrium radionuclide angiography. In: Heller GV, Hendel RC, editors. Nuclear cardiology: Practical application. New York: McGraw-Hill; 2004.p.103-117.

28. Patton JA. Physics principles and instrumentation in nuclear cardiology. In: Vitola JV, Delbeke D, editors. Nuclear cardiology and correlative imaging. New York: Springer; 2004. p.13-48.

29. Equilibrium gated blood pool [homepage on the Internet] date unknown [cited 2005 Aug 17] Available from: URL:http://www.tmc.edu/thi/dimuga.html

30. Maine TJ, Hanson MW, Borges-Neto S. The additive value of combined assessment of myocardial perfusion and ventricular function studies. J Nucl Med.2004;45:1721-24.

31. Paul AK, Nabi HA. Gated myocardial perfusion SPECT: basic principles, technical aspects, and clinical applications. J Nucl Med Technol.2004;32:179-87.

32. Heller GV, Navare S. Interpretation of ventricular function using ECG-gated SPECT imaging. In: Heller CV, Hendel RC, editors. Nuclear cardiology: practical applications. New York: McGraw-Hill; 2004. p.175-185

33. Available from: URL: http://brighamrad.hardvard.edu/education/online/cardiac/Gated-SPECT.html.

34. Go V, Bhatt MR, Hendel RC. The diagnostic and prognostic value of ECG-gated SPECT myocardial perfusion imaging. J Nucl Med.2004;45:912-21.

35. Germano G, Kiat H, Kavanagh PB, Moriel M, Mazzanti Marco, Te Su H, et al. Automatic quantification of ejection fraction from gated myocardial perfusion SPECT. J Nucl Med 1995;36:2138-47.

36. Faber TL, Cooke CD, Folks RD, Vansant JP, Nichols KJ, DePuey EG, et al. Left ventricular function and perfusion from gated SPECT perfusion images: an integrated method. J Nucl Med. 1999; 40:650-59.

37. Faber TL, Cooke CD, Peifer JW, Pettigrew RI, Vansant JP, Leyendecker JR, et al. Three-Dimensional displays of left ventricular epicardial surface from standard cardiac SPECT perfusion quantification techniques. J Nucl Med.1995;36:697-703.

38. 4D-MSPECT manual

39. Zeng GL. Image reconstruction-a tutorial. Computerized Medical Imaging and Graphics. 2001;25:97-103.

40. Bruyant PP. Analytic and iterative reconstruction algorithms in SPECT. J Nucl Med.2002;43:1343-58.

41. Boellaard R, Lingen A, Lammertsma AA. Experimental and clinical evaluation of iterative reconstruction (OS-EM) in dynamic PET: Quantitative characteristics and effects on kinetic modeling. J Nucl Med 2001; 42: 808-17.

42. Tocharoenchai C.Optimization of the coincidence energy window setting for a hybrid PET system using an LROC study. Ph.D.dissertation. The University of North Carolina at Chapel Hill, 2001.

43. Hudson HM, Larkin RS. Accelerated image reconstruction using ordered subsets of projection data. IEEE Trans Med Imaging. 1994; 13: 601-09.

44. Lalush DS. The application of a Gibbs prior with a generalized potential function to maximum a posteriori SPECT reconstruction. Ph. D. dissertation. The university of North Carolina at Chapel Hill, 1992.

45. Lalush DS, Tsui BMW. Performance of ordered-subset reconstruction algorithms under conditions of extreme attenuation and truncation in myocardial SPECT. J Nucl Med.2000;41:737-44.

46. Vallejo E, Dione DP, Sinusas AJ, Wackers F. Assessment of left ventricular ejection fraction with quantitative gated SPECT: accuracy and correlation with first-pass radionuclide angiography. J Nucl Cardiol 2000; 7: 461-70.

47. Gayed I, Cid E, Boccalandero F, Podoloff D. Factor affecting left ventricular ejection fraction using automated quantitative gated SPECT. Clinical nuclear medicine 2003; 28: 290-95.

48. Nakajima K, Higuchi T, Taki J, Kawano M, Tonami N. Accuracy of ventricular volume and ejection fraction measured by gated myocardial SPECT: comparison of 4 software programs. J Nucl Med 2001; 42: 1571-78.

49. Cherry SP, Sorenson JA, Phelps ME. Physics in nuclear medicine. 3rd ed. Philadelphia; Elsevier Science.2003.p.131-48.

50. Vallejo E, Dione DP, Bruni WL, Constable RT, Borek PP, Soares JP, et al. Reproducibility and accuracy of gated SPECT for determination of left ventricular volumes and ejection fraction: Experimental validation using MRI. J Nucl Med 2000; 41:874-82.

51. Shaefer WM, Lipke C, Standke D, Kuhl HP, Nowak B, Kaiser H, et al. Quantification of left ventricular volumes and ejection fraction from gated ^{99m}Tc-MIBI SPECT: MRI validation and comparison of the Emory Cardiac Toolbox with QGS and 4D-MSPECT. J Nucl Med 2005;46:1256-63.

52. Faber TL, Vansant JP, Pettigrew RI, Galt JR, Blais M, Chatzimavroudis G, et al. Evaluation of left ventricular endocardial volumes and ejection fractions computed from gated perfusion SPECT with magnetic resonance imaging: comparison of two methods. J Nucl Cardiol 2001;8:645-51.

53. Lum DP, Coel MN. Comparison of automatic quantification software for the measurement of ventricular volume and ejection fraction in gated myocardial perfusion SPECT. Nuclear Medicine Communications. 2003;24:259-66.

54. Liow JS, Strother SC, Rehm K, Rottenberg DA. Improved resolution for PET volume imaging through three-dimensional iterative reconstruction. J Nucl Med. 1997;38:1623-31.

BIOGRAPHY

NAME	Miss. Oranuch Tiapetch
DATE OF BIRTH	15 August 1981
PLACE OF BIRTH	Suphanburi, Thailand
INSTITUTIONS ATTENDED	Mahidol University, 2003 : Bachelor of Science (Radiological Technology) Mahidol University, 2006 : Master of Science (Medical Physics)
HOME ADDRESS	171/455 Somdejphrapinklao Rd., Arun-Amarin, Bangkoknoi, Thailand 10700 Tel. 02-4343697, 06-0489022 Email : kookai2524@hotmail.com